Behavior and design of high-strength steel columns under combined compression and bending

8

Kwok-Fai Chung[1], *Tian-Yu Ma*[1,2], *Guo-Qiang Li*[2] *and Xiao-Lei Yan*[2]
[1]Hong Kong Polytechnic University, Hong Kong, P.R. China, [2]Tongji University, Shanghai, P.R. China

8.1 Introduction

This chapter presents both experimental [1,2] and numerical investigations [2,3] on high-strength steel (HSS) columns under combined compression and bending. Two types of sections, including welded H-sections and welded box-sections, are considered for the columns. In the experimental investigation, a total of eight columns of welded H-sections made of Q690 steel and a total of seven columns of welded box-sections made of Q460 steel were tested under eccentric loads. Initial out-of-straightness of these columns was measured during the preparation of the test, and initial loading eccentricity was acquired by different methods. In the test process, applied load, local strain, axial deformation, and lateral deflection were obtained. All the columns failed by overall buckling. The buckling resistances measured in these tests were compared to their corresponding design results according to different design codes. Then, numerical investigations were performed by using finite element models. Geometrical and material nonlinearities were incorporated in these finite element (FE) models, and these models showed excellent capability of replicating the key test data. Upon validation of the FE models, parametric studies were conducted to evaluate different effects influencing buckling resistances of HSS columns of welded sections. Afterward, applicability of design rules on steel columns under combined compression and bending given in different design codes is assessed by means of the ratios of the FE to design buckling resistances. And design proposals on HSS columns under combined compression and bending were made.

Behavior and Design of High-Strength Constructional Steel. DOI: https://doi.org/10.1016/B978-0-08-102931-2.00008-5

8.2 Experimental investigation

8.2.1 H-sections

8.2.1.1 Test program

A total of eight slender columns of welded H-sections were tested under combined compression and bending about minor axis of their cross sections. These columns were made from high-strength Q690 steel plates with nominal thicknesses of 6, 10, and 16 mm. Four sections of different cross-sectional dimensions, Sections H1, H2, H3, and H4, were involved. Their nominal dimensions and section classifications according to EN 1993-1-1 and ANSI/AISC 360-16 are shown in Fig. 8.1, while their measured dimensions and section properties are summarized in Table 8.1.

8.2.1.2 Specimen fabrication

All the specimens were fabricated under the following steps:

- Cut the steel plates into strips and assemble them to form H-sections with tack welds.
- A preheating of 120°C was applied to web-to-flange junctions to facilitate good quality welding.
- For each section the web was connected to the flanges with fillet welds on both sides of the web. Gas metal arc welding (GMAW) with a fillet size of 6 mm was used for Sections H1 and H2, while submerged arc welding (SAW) with a fillet size of 10 mm was used for Sections H3 and H4. The fillet sizes were assigned to be the same as the web thicknesses to ensure structural adequacy. Each fillet was formed in a single run that was staggered with a length of 500−600 mm along the column length to minimize distortion due to welding. Technical information on electrodes and welding parameters are shown in Table 8.2. Since the electrical parameters fluctuated during welding, average values were taken.

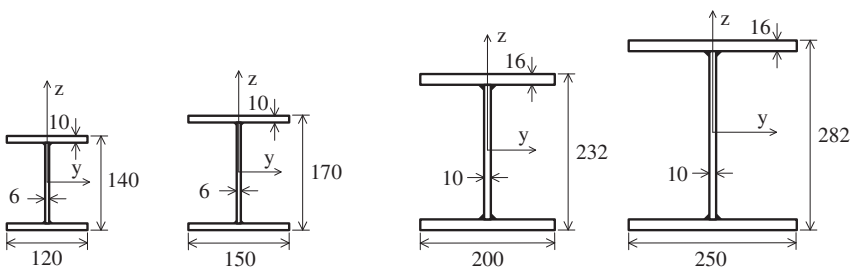

Figure 8.1 Nominal cross-sectional dimensions of welded H-sections: (A) Section H1, (B) Section H2, (C) Section H3, and (D) Section H4.

Table 8.1 Measured dimensions and section properties of welded H-sections.

Test	Section depth	Section width	Flange thickness	Web thickness	Specimen length	Effective length	Area	Second moment of area	Radius of gyration
	H	b	t_f	t_w	L_s	L_{eff}	A	I_z	i_z
	(mm)	(mm)	(mm)	(mm)	(mm)	(mm)	(mm^2)	($\times 10^6$ mm^4)	(mm)
EH1P	140.0	119.6	9.90	5.83	1612	1992	3070	2.83	30.4
EH1Q	141.2	119.8	9.91	5.85	2410	2790	3085	2.84	30.3
EH2P	170.0	149.3	9.90	5.81	1613	1993	3827	5.49	37.9
EH2Q	170.0	149.7	9.92	5.85	2410	2790	3847	5.54	38.0
EH3P	231.8	201.5	15.98	9.92	1613	1993	8422	21.81	50.9
EH3Q	231.7	200.7	15.97	9.95	2412	2792	8397	21.54	50.6
EH4P	284.2	250.1	15.97	9.92	1611	1991	10490	41.66	63.0
EH4Q	282.0	249.9	15.93	9.93	2410	2790	10448	41.47	63.0

Table 8.2 Information on welding electrodes and welding parameters.

Section	Welding method	Welding electrodes				Welding parameters			
		Product designation	Diameter (mm)	Yield strength (N/mm^2)	Tensile strength (N/mm^2)	Voltage (V)	Current (A)	Speed (mm/s)	Fillet size (mm)
H1 and H2	GMAW	CHW-80C1	1.2	660	760	30	240	4.1	6
H3 and H4	SAW	CHW-S80	4.0	680	760	36	450	6.1	10

GMAW, Gas metal arc welding; *SAW*, submerged arc welding.

- After the H-sections were assembled, a pair of Q345 steel 30 mm thick end plates was welded onto both ends of the H-sections. Triangular stiffeners were welded to strengthen the connections between end plates and flanges.

8.2.1.3 Material properties

To obtain the material properties of Q690 steel plates, a total of nine tensile tests were carried out. The stress−strain curves for all the tensile tests are plotted in Fig. 8.2. It is found that for all the Q690 steel plates with different thickness, no definite yielding plateau is observed, and strain hardening started shortly after occurrence of yielding. The measured material properties are summarized in Table 8.3.

It should be noted that EN 1993-1-12 specifies the following ductility criteria for steel materials with steel grades from S460 up to S700: (1) $f_u/f_y \geq 1.05$, (2) elongation at failure not less than 10%, and (3) $\varepsilon_u \geq 15\ f_y/E$. It is shown that all the steel plates satisfy these ductility criteria, and they are readily qualified to be HSS materials to EN 1993-1-12.

8.2.1.4 Test setup

All the tests were conducted with a 1000 t universal servo-controlled testing machine, and the general test setup is shown in Fig. 8.3. A pair of attachments was connected to both ends of the H-sections through bolts. These attachments provided an eccentricity of about 100 mm along the minor axis of the H-sections for the applied compressive loads. And they also enabled the H-sections to rotate freely at both ends about the minor axis of the H-sections. Therefore these columns were tested under combined compression and bending.

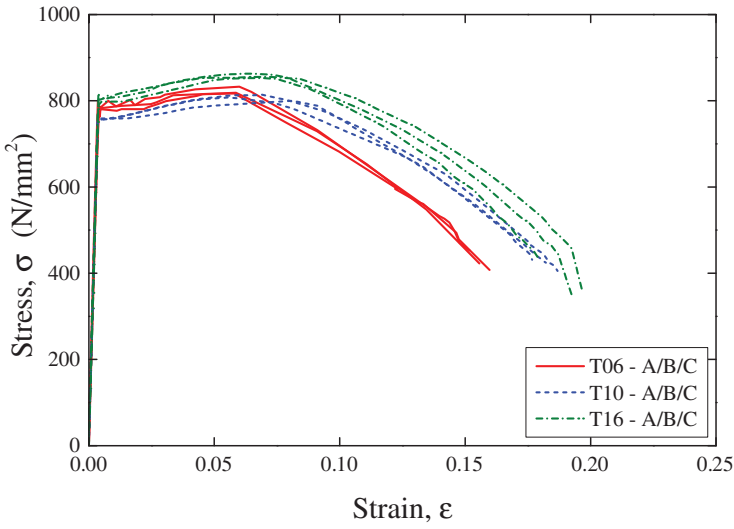

Figure 8.2 Stress−strain curves of Q690 steel plates.

Table 8.3 Mechanical properties of Q690 steel plates.

Nominal thickness t (mm)	Coupon	Young's modulus E (kN/mm^2)	Yield strength f_y (N/mm^2)	Tensile strength f_u (N/mm^2)	Ratio f_u/f_y	Strain at f_u ε_u	Elongation at fracture A (%)
6	T06-A	210	771	819	1.06	0.059	15.5
	T06-B	210	764	810	1.06	0.060	15.3
	T06-C	209	763	817	1.07	0.058	16.0
	Average	210	766	815	1.06	0.059	15.6
10	T10-A	212	753	788	1.05	0.065	18.2
	T10-B	214	758	796	1.05	0.078	18.9
	T10-C	211	756	794	1.05	0.067	18.7
	Average	212	756	793	1.05	0.070	18.6
16	T16-A	208	800	855	1.07	0.064	19.7
	T16-B	206	797	833	1.05	0.065	17.9
	T16-C	212	804	843	1.05	0.068	19.3
	Average	209	800	844	1.05	0.066	19.0

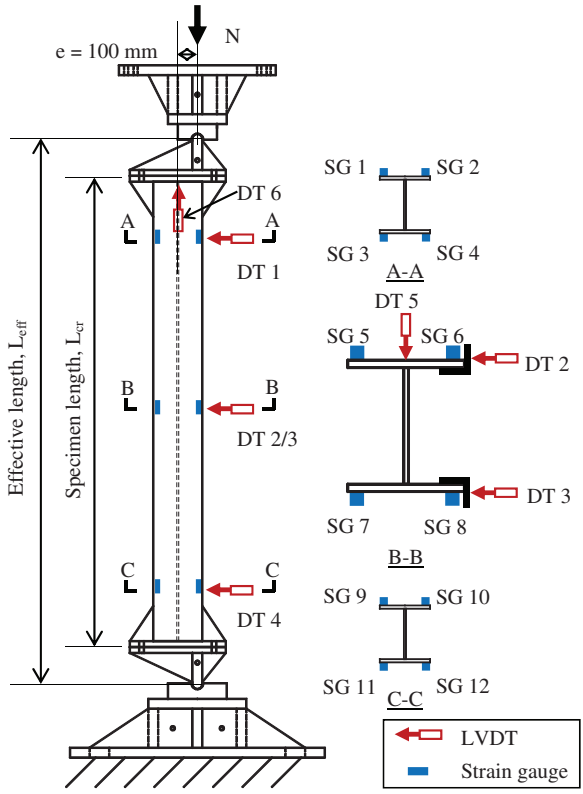

Figure 8.3 Test setup for welded H-sections under eccentric loads.

A total of 12 strain gauges were mounted onto the outer surfaces of the flanges of the H-sections at three cross sections, namely, Sections A−A, B−B, and C−C. At each section, four strain gauges were installed 10 mm away from the edges of the flanges. Displacement transducers DT1, DT2, DT3, and DT4 were used to measure lateral deflections of the H-sections at these three sections along the direction of the major axis of their cross sections. It should be noted that any difference in the measurements between Transducers DT2 and DT3 would give a twisting of the H-sections along their longitudinal axes. Transducer DT5 was used to capture any lateral deflection of the H-section along the minor axis at Section B−B for a monitoring purpose while Transducer DT6 was used to measure axial deformations of the H-sections.

8.2.1.5 Initial out-of-straightness

Before testing, initial out-of-straightness of each H-section was measured. A steel wire was attached to the surface of one flange of the H-section, and it ran through the centerline of the flange from Sections A−A to C−C. Any deviation of the flange at the midheight of the H-section was regarded as the initial out-of-straightness of this

flange, denoted as v_1. Measurement was repeated on the other flange to obtain v_2. The average value of v_1 and v_2 was considered to be the initial out-of-straightness of the H-section, denoted as v. The initial out-of-straightness for all the H-sections is summarized in Table 8.4. Due to limitations of this measuring method, any initial out-of-straightness smaller than the radius of the steel wire, that is, 0.25 mm, could not be recognized, and this situation is denoted with "−." It is shown that the absolute values of the measured out-of-straightness of all the H-sections are smaller than 1.0 mm, also far away from 1/1000 of their effective lengths, L_{eff}. Thus these initial out-of-straightnesses would have very little effects on buckling behavior of the H-sections. In general, quality of the workmanship in fabricating these high-strength Q690 steel welded H-sections was considered to be high and readily achieved in modern fabrication shops.

8.2.1.6 Test procedures

In the initial stage of testing a load was applied at a loading rate of 30−105 kN/min onto the H-sections, depending on their cross-sectional areas. Under this loading condition the average stress rate for each H-section was kept to be smaller than 10 N/mm^2/min. This loading rate was maintained until 80% of the predicted (or designed) buckling resistances of each H-section were attained. The calculation of the predicted buckling resistances will be discussed later. Then, a displacement control was adopted with a deformation rate of 0.5 mm/min. Under this displacement rate the average strain rate for each H-section was smaller than 0.00025/min, and hence, these tests should be regarded as static tests. The tests terminated after the applied load attained its maximum value and dropped down to 85% of the maximum value.

8.2.1.7 Test results

Failure modes and failure loads

All the H-sections failed in overall flexural buckling about minor axis of their cross sections, as shown in Fig. 8.4. The maximum applied load observed in each test

Table 8.4 Initial out-of-straightness at midheight of welded H-sections.

Test	v_1 (mm)	v_2 (mm)	$v = (v_1 + v_2)/2$ (mm)	L_{eff} (mm)	$\lvert v\rvert/L_{eff}$ ($\times 10^{-3}$)
EH1P	–	+ 0.3	+ 0.2	1992.0	0.1
EH1Q	− 0.5	− 0.5	− 0.5	2790.1	0.2
EH2P	+ 0.2	–	+ 0.1	1993.3	0.1
EH2Q	− 0.5	− 0.5	− 0.5	2790.3	0.2
E3HP	–	–	0	1993.3	0.0
E3HQ	− 1.5	− 0.5	− 1.0	2791.6	0.4
E4HP	− 0.5	− 0.5	− 0.5	1990.5	0.3
E4HQ	–	–	0	2790.1	0.0

Notes: (1) "−" represents a value smaller than 0.25, and it may be taken to be 0. (2) The signs of these values indicate the positions of the deviations.

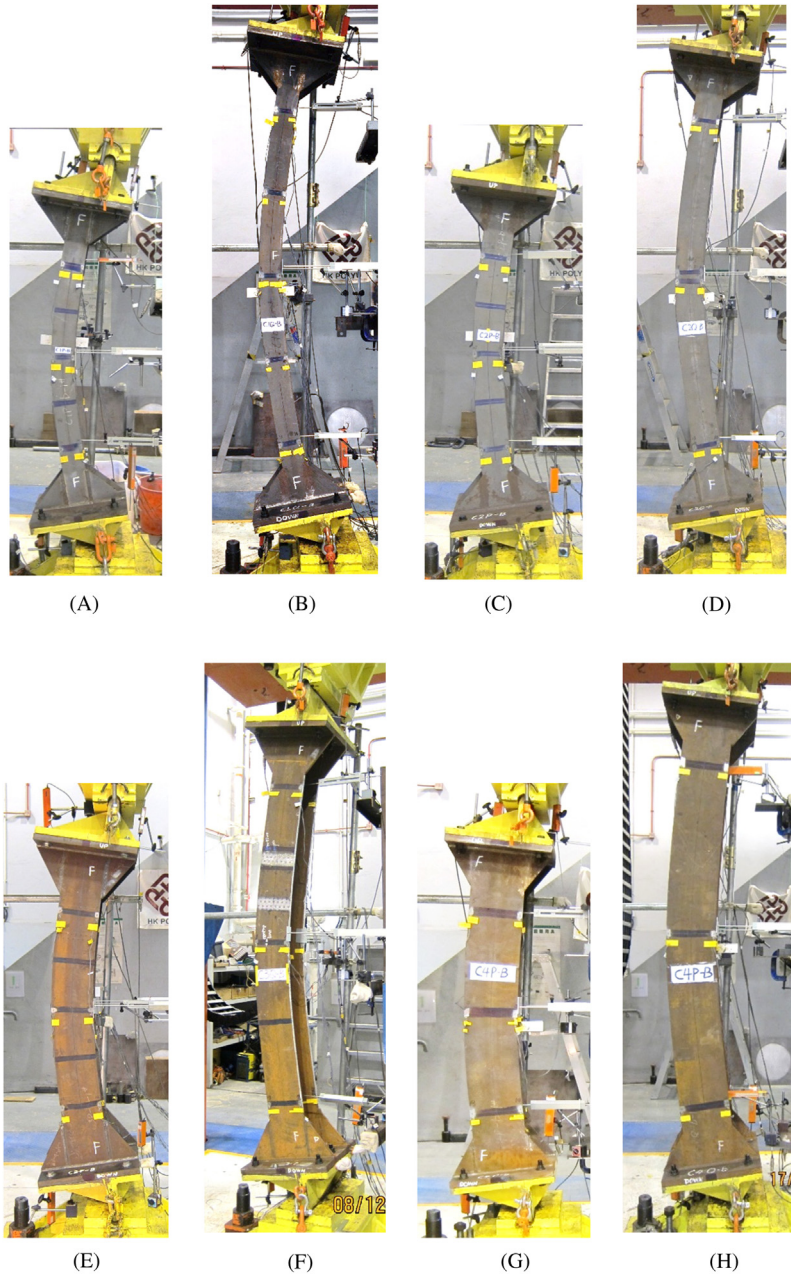

Figure 8.4 Overall flexural buckling of welded H-sections under eccentric loads: (A) test EH1P, (B) test EH1Q, (C) test EH2P, (D) test EH2Q, (E) test EH3P, (F) test EH3Q, (G) test EH4P, and (H) test EH4Q.

was regarded as the measured buckling resistance of the corresponding column, as summarized in Table 8.5.

Load–deformation relationships

For all welded H-sections, lateral deflections of the flanges at midheight were recorded by Transducers DT2 and DT3. Hence, the average values of these two transducer readings were regarded as the lateral deflections, Δy, of the welded H-sections. The relationships between the applied load, N, and the lateral deflection, Δy, of all welded H-sections are shown in Fig. 8.5. It should be noted that the maximum differences between these two transducer readings were found to be smaller than 0.2 mm throughout the testing, and hence, twisting of the H-sections at midheight of the welded H-sections was considered to be insignificant in the present tests.

Moreover, axial deformations of the welded H-sections, Δx, were measured with Transducer DT6. The relationships between the applied load, N, and the axial deformation, Δx, of all the welded H-sections are shown in Fig. 8.6.

It is shown that both the lateral deflections, Δy, and the axial deformations, Δx, increase almost linearly with an increase of the applied load, N, up to failure in all tests. After the failure loads, N_{test}, were attained, unloading took place gradually with further deformations in all the welded H-sections. In general, all of these load–deformation relationships are considered to be similar to those slender columns of welded H-sections made of conventional steel materials.

Load–strain relationships

For each H-section, there were a total of 12 strain gauges mounted onto the outer surfaces of their two flanges, and these strain gauges were divided into a group of 4 strain gauges at three different cross sections, Sections A–A, B–B, and C–C. It is interesting to plot development of these axial strains measured at these three cross sections during load application. Fig. 8.7 plots relationships between the applied load, N, and the axial strains, ε_x, at various cross sections of test EH3P for easy comparison. It should be noted that under the presence of combined compression and bending at midheight of the welded H-section, that is, Section B-B, measured resultant axial stresses from strain gauges SG 6 and 8 are found to be in compression while those from strain gauges SG 5 and 7 are in tension. As the applied load increases, the strain readings of

Table 8.5 Measured buckling resistances of welded H-sections.

Test	N_{test} (kN)	$\overline{\lambda}_z$	λ_z
EH1P	328	1.26	66
EH1Q	250	1.77	92
EH2P	527	1.01	53
EH2Q	418	1.42	74
EH3P	1698	0.77	39
EH3Q	1376	1.08	55
EH4P	2662	0.62	32
EH4Q	2276	0.87	44

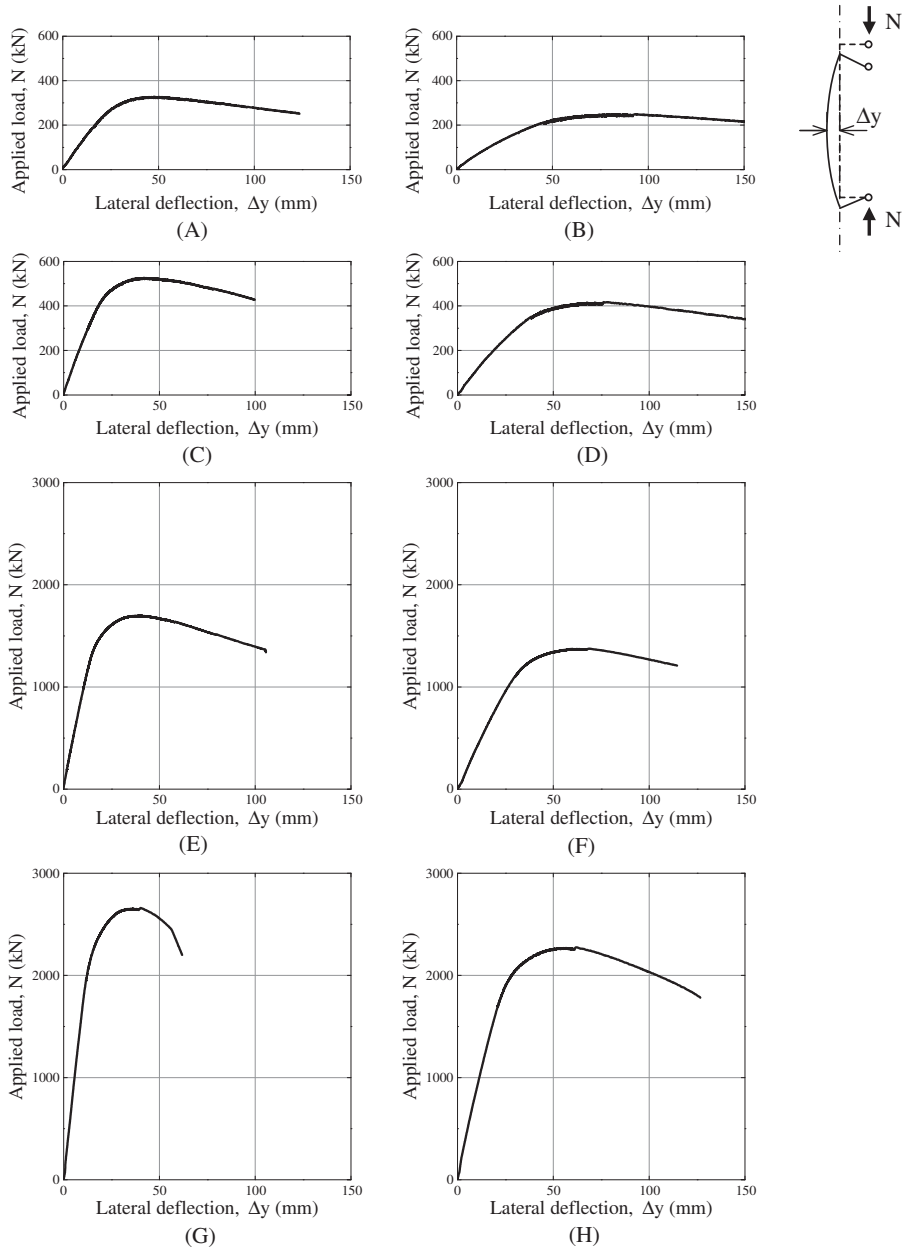

Figure 8.5 Relationships between applied loads and lateral deflections for welded H-sections under combined compression and bending: (A) test EH1P, (B) test EH1Q, (C) test EH2P, (D) test EH2Q, (E) test EH3P, (F) test EH3Q, (G) test EH4P, and (H) test EH4Q.

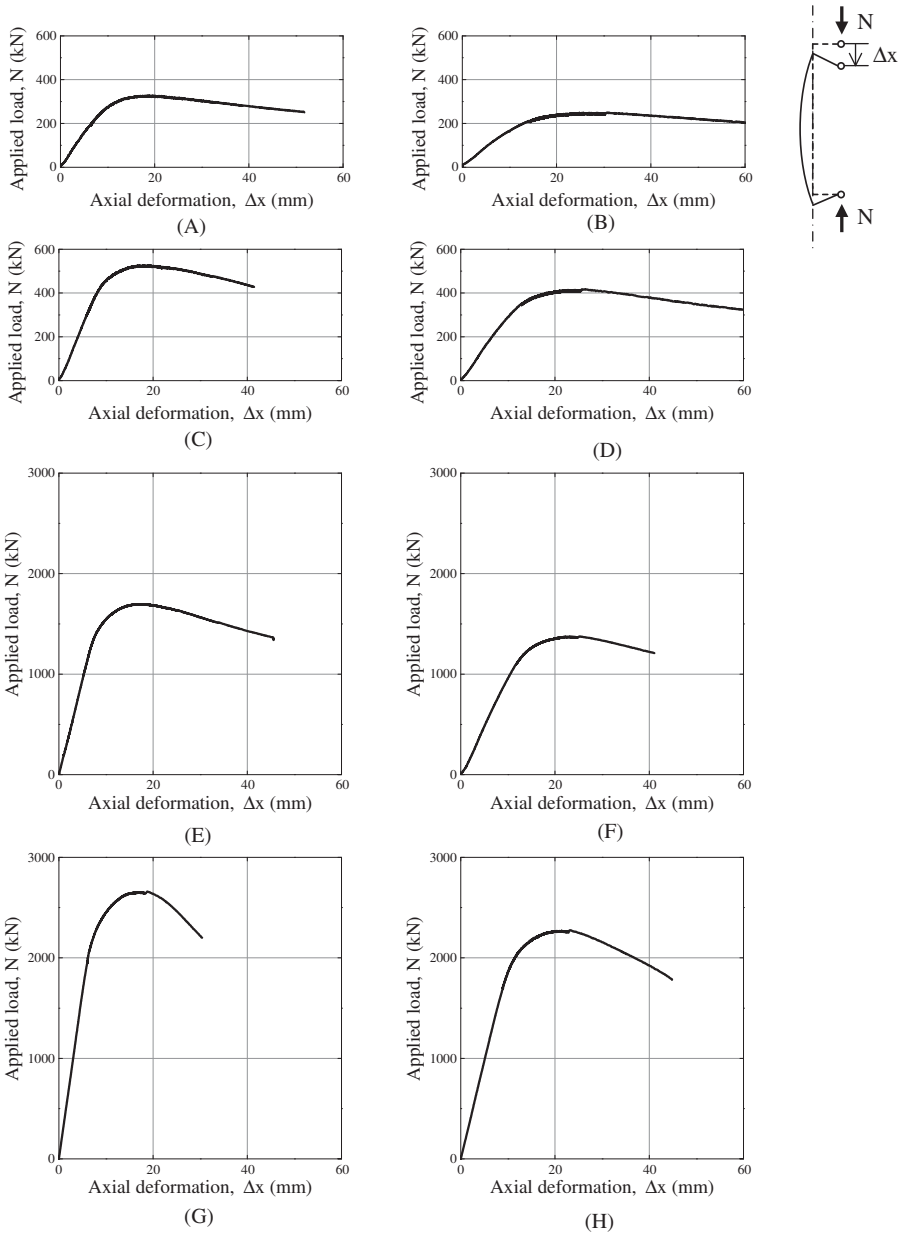

Figure 8.6 Relationships between applied loads and axial deformations for welded H-sections under combined compression and bending: (A) test EH1P, (B) test EH1Q, (C) test EH2P, (D) test EH2Q, (E) test EH3P, (F) test EH3Q, (G) test EH4P, and (H) test EH4Q.

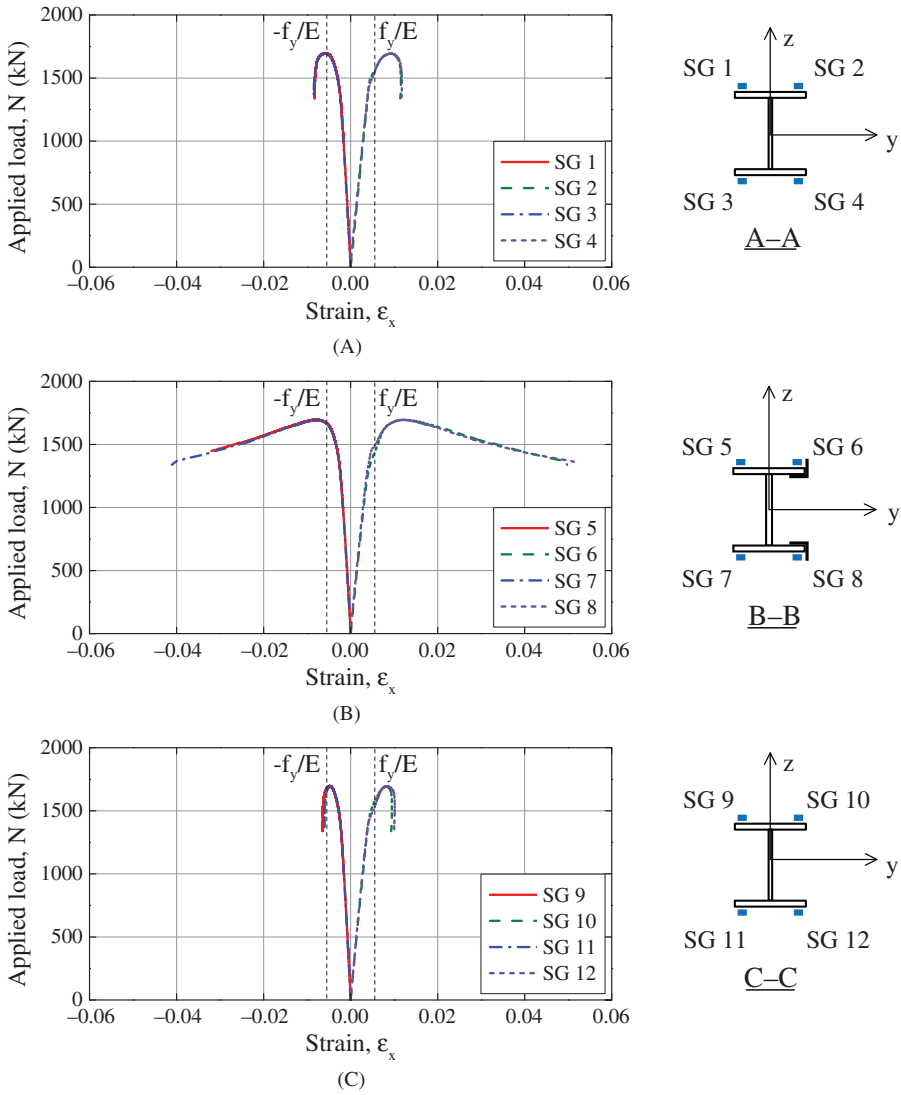

Figure 8.7 Relationships between applied load and axial strains of welded H-sections—test EH3P: (A) Section A−A, (B) Section B−B, and (S) Section C−C.

these four strain gauges exceed the value of the yield strain, ε_y(or f_y /E). Hence, yielding occurs, leading the H-section to fail in an elastoplastic manner.

Initial loading eccentricity

The initial loading eccentricities at Section A−A, e_A, and Section C−C, e_C, are defined as the eccentricities of the rotation centers at the H-section ends with respect to the line passing through the centerline of the flange at Sections A−A and C−C before loading,

respectively, as shown in Fig. 8.8. The measured initial loading eccentricities, e_A and e_C, for the welded H-sections in an elastic stage were obtained by using the applied load readings, and the corresponding strain readings and lateral deflections under the applied load at Sections A−A and C−C, respectively. For Section A−A the strain distribution of the whole cross section was obtained using strain readings measured by strain gauges SG5, SG6, SG7, and SG 8. The stress distribution at this cross section was then obtained by using the stress−strain curves obtained from the coupon tests, and hence, the corresponding internal moment under the applied load, $M_{A,SG}$, was computed accordingly. Consequently, the initial loading eccentricity at Section A−A, e_A, was readily obtained through equilibrium consideration as follows:

$$e_A = \frac{M_{A,SG}}{N} - d_A \tag{8.1}$$

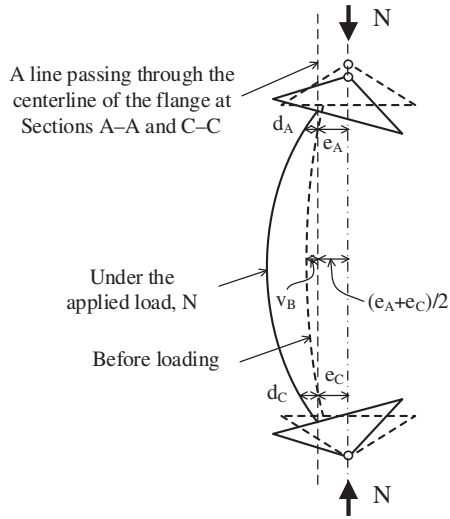

Figure 8.8 Measurement of loading eccentricity.

Table 8.6 Loading Eccentricities of all the welded H-sections.

Test	Section A−A e_A (mm)	Section C−C e_C (mm)	Average $(e_A + e_C)/2$ (mm)
EH1P	+ 101.5	+ 101.4	+ 101.5
EH1Q	+ 96.4	+ 95.8	+ 96.1
EH2P	+ 106.0	+ 101.6	+ 103.8
EH2Q	+ 98.4	+ 101.0	+ 99.7
E3HP	+ 100.1	+ 96.2	+ 98.2
E3HQ	+ 101.9	+ 102.9	+ 102.4
E4HP	+ 97.8	+ 102.3	+ 100.1
E4HQ	+ 99.1	+ 98.0	+ 98.6

where N is the applied load in the initial loading stage, d_A is the corresponding lateral deflection at Section A−A under the applied load, N. The initial loading eccentricity at Section C−C, e_C, was obtained from a similar process. Table 8.6 summarizes the initial loading eccentricities of all the welded H-sections. The average value of the initial loading eccentricities of each welded H-section was employed to calculate the first order applied moment in subsequent analyses and calibration.

8.2.1.8 Applicability of design rules

Applicability of design rules given in EN 1993-1-1, ANSI/AISC 360-16, and GB 50017-2003 for welded H-sections under combined compression and bending is assessed through calibration against the test results. In these design rules the effects of axial compression and bending moments are summed up linearly, while nonlinear effects of applied bending moments are accounted for by interaction factors. In general, two formulae should be satisfied, each of which corresponds to member buckling about a principal plane. However, as there was no applied moment about the major axis of the cross sections of the H-sections, lateral-torsional buckling did not occur in the tests. Hence, the critical formula is the one corresponding to flexural buckling of the H-sections under bending about minor axis.

EN 1993-1-1

According to EN 1993-1-1, members who are subjected to combined compression and bending should satisfy the following equations:

$$\frac{N_{Ed}}{\chi_y N_{Rk}/\gamma_{M1}} + k_{yy}\frac{M_{y,Ed}+\Delta M_{y,Ed}}{\chi_{LT}\left(M_{y,Rk}/\gamma_{M1}\right)} + k_{yz}\frac{M_{z,Ed}+\Delta M_{z,Ed}}{M_{z,Rk}/\gamma_{M1}} \le 1 \tag{8.2}$$

$$\frac{N_{Ed}}{\chi_z N_{Rk}/\gamma_{M1}} + k_{zy}\frac{M_{y,Ed}+\Delta M_{y,Ed}}{\chi_{LT}\left(M_{y,Rk}/\gamma_{M1}\right)} + k_{zz}\frac{M_{z,Ed}+\Delta M_{z,Ed}}{M_{z,Rk}/\gamma_{M1}} \le 1 \tag{8.3}$$

where N_{Ed}, $M_{y,Ed}$, and $M_{z,Ed}$ are the design values of the compression force and the moments about the major (y) and the minor (z) axes along the member, respectively; N_{Rk}, $M_{y,Rk}$, and $M_{z,Rk}$ are the characteristic values of resistances to compression force and the bending moments about the major (y) and the minor (z) axes, respectively; $\Delta M_{y,Ed}$ and $\Delta M_{z,Ed}$ are the moments due to the shift of the centroidal axes for Class 4 sections; χ_y and χ_z are the reduction factors due to flexural buckling about the major (y) and the minor (z) axes, respectively; χ_{LT} is the reduction factor due to lateral-torsional buckling; k_{yy}, k_{yz}, k_{zy}, and k_{zz} are the interaction factors; and γ_{M1} is the partial factor for resistance of members to instability assessed by member checks.

The reduction factors χ_y and χ_z in the first terms in Eqs. (8.2) and (8.3) are determined by a suitable selection of flexural buckling curves. According to the complementary rules in EN 1993-1-12 for high-strength Q690 steel welded H-sections, a curve "c" is recommended to calculate the flexural buckling resistances of

the H-sections for buckling about the minor axis of the cross sections. The interaction factors k_{yy}, k_{yz}, k_{zy}, and k_{zz} in the second and the third terms may be obtained from two different approaches given in Annexes A and B, respectively. It should be noted that the main difference between these two approaches is the way of presenting different structural effects. As Annex A emphasizes transparency, each structural effect is accounted for by an individual factor. However, Annex B works with simplicity and allows some structural effects to be combined into a global factor. Based on these two approaches, the design resistances $N_{EC3,c}$ for all the H-sections were calculated through iterations.

In the calculations, measured dimensions and mechanical properties as well as total initial geometrical imperfections were adopted. All the moment resistances of the H-sections are given by their plastic moduli even though Sections H2 and H4 are considered to be merely Class 3 sections. Table 8.7 summarizes both the failure loads N_{test} and the design resistances $N_{EC3,c}$ of the H-sections. It should be noted that:

- According to the approach given in Annex A, the values of $N_{test}/N_{EC3,c}$ are found to range from 1.06 to 1.11 with an average value of 1.09.
- According to the approach given in Annex B, the values of $N_{test}/N_{EC3,c}$ are found to range from 1.10 to 1.24 with an average value of 1.20.

Comparison between the test and the design resistances may be illustrated through plotting test values onto the graphs of normalized interaction curves according to the approaches in Annexes A and B for each of the four H-sections in Fig. 8.9. As shown in the graphs, Annex B tends to give more conservative results when compared with Annex A.

It should be noted that in order to improve structural efficiency of the design rules, curve "a" is suggested to be used in the flexural buckling design of the welded H-sections to give the axial buckling resistances $N_{EC3,a}$ of the sections under combined compression and bending. The values of $N_{EC3,a}$ are also summarized in Table 8.7 for direct comparison with those of $N_{EC3,c}$. It should be noted that:

- According to the approach given in Annex A, the values of $N_{test}/N_{EC3,a}$ are found to range from 1.02 to 1.07 with an average value of 1.05.
- According to the approach given in Annex B, the values of $N_{test}/N_{EC3,a}$ are found to range from 1.03 to 1.16 with an average value of 1.11.

Hence, by selecting a proper parameter in designing flexural resistances of the H-sections, the approaches in both Annexes A and B are shown to be significantly improved in giving conservative and yet efficient resistances for high-strength Q690 steel welded H-sections under combined compression and bending about minor axis. The use of curve "a" in designing flexural resistances of welded H-sections is also supported by other researchers as structural effects of residual stresses are proportionally less pronounced in these sections, when compared with those of conventional steel materials.

Table 8.7 Calibration of EN 1993-1-1 for Q690 steel welded H-sections under combined compression and bending.

Test	N_{test} **(kN)**	λ	$\overline{\lambda}$	**EN 1993-1-1: Annex A**				**EN 1993-1-1: Annex B**			
				$N_{EC3,c}$ **(kN)**	$N_{test}/N_{EC3,c}$	$N_{EC3,a}$ **(kN)**	$N_{test}/N_{EC3,a}$	$N_{EC3,c}$ **(kN)**	$N_{test}/N_{EC3,c}$	$N_{EC3,a}$ **(kN)**	N_{test}/N
EH1P	328	66	1.26	295	1.11	306	1.07	272	1.21	293	1.12
EH1Q	250	92	1.77	231	1.08	240	1.04	227	1.10	238	1.05
EH2P	527	53	1.01	477	1.10	495	1.07	425	1.24	461	1.14
EH2Q	418	74	1.42	386	1.08	402	1.04	362	1.15	393	1.06
EH3P	1698	39	0.77	1599	1.06	1666	1.02	1424	1.19	1523	1.12
EH3Q	1376	55	1.08	1250	1.10	1310	1.05	1129	1.22	1238	1.11
EH4P	2662	32	0.62	2481	1.07	2579	1.03	2185	1.22	2303	1.16
EH4Q	2276	44	0.87	2075	1.10	2179	1.04	1848	1.23	2018	1.13
Average	–	–	–	–	1.09	–	1.05	–	1.20	–	1.11

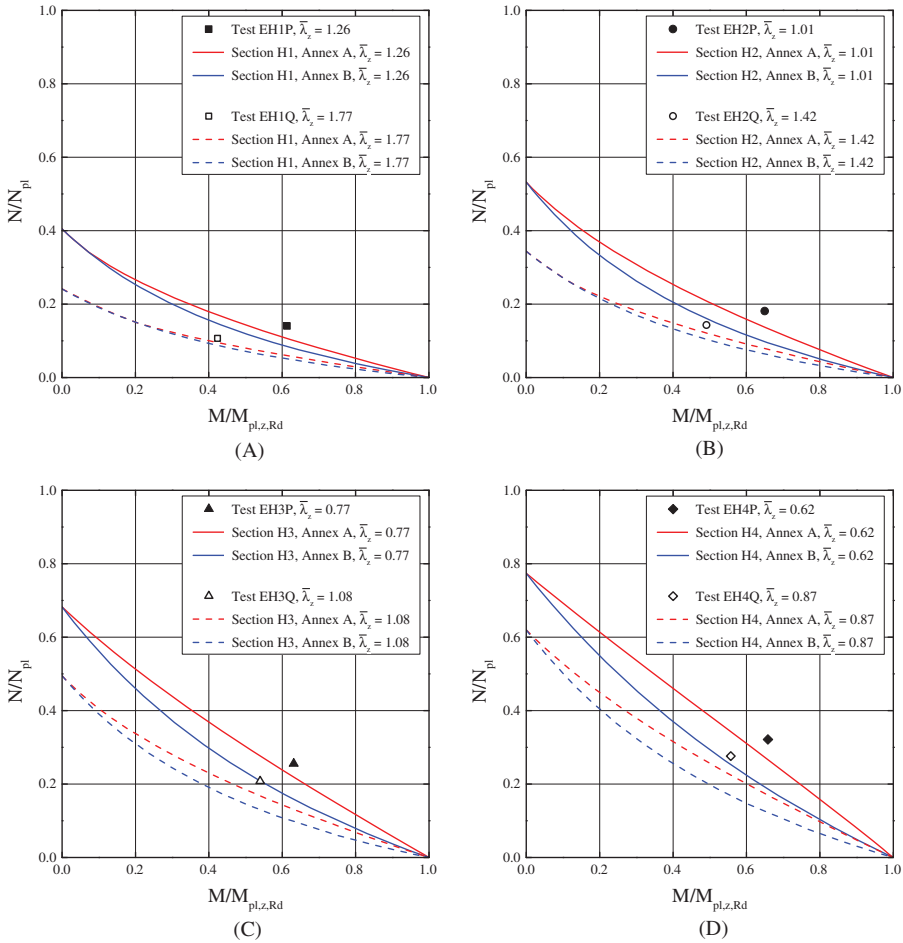

Figure 8.9 Normalized interaction curves to EN 1993-1-1: (A) Section H1, (B) Section H2, (C) Section H3, and (D) Section H4.

ANSI/AISC 360-16

ANSI/AISC 360-16 is applicable to steel grades up to 690 N/mm^2 (ASTM A514 and A709 steel). For doubly and singly symmetric members subject to combined compression and bending, the following equations in ANSI/AISC 360-16 should be satisfied:

$$\text{When } \frac{P_r}{P_c} \geq 0.2 \quad \frac{P_r}{P_c} + \frac{8}{9}\left(\frac{M_{rx}}{M_{cx}} + \frac{M_{ry}}{M_{cy}}\right) \leq 1.0 \tag{8.4}$$

$$\text{When } \frac{P_r}{P_c} < 0.2 \quad \frac{P_r}{2P_c} + \left(\frac{M_{rx}}{M_{cx}} + \frac{M_{ry}}{M_{cy}}\right) \leq 1.0 \tag{8.5}$$

where P_r is the design axial force, P_c is the axial buckling resistance, M_{rx} and M_{ry} are the design moments about the major (x) and the minor (y) axes, respectively, and M_{cx} and M_{cy} are the moment resistances about the major (x) and the minor (y) axes, respectively.

It should be noted that the design axial forces, $P_{r,ANSI}$, for all the H-sections are calculated through iterations. Comparison between the test resistances N_{test} and the design resistances $P_{r,ANSI}$ is shown in Table 8.8, and corresponding normalized interaction curves are plotted in Fig. 8.10. It is found that the design rules in ANSI/AISC 360-16 tend to provide close but slightly unconservative predictions to the failure loads of high-strength Q690 steel welded H-sections under combined compression and bending about minor axis.

GB 50017-2003

It should be noted that Q690 steel is beyond the scope of GB 50017-2003, and hence, it is necessary to verify its applicability to design Q690 steel materials. For members under combined compression and bending, the following equations in GB 50017-2003 should be satisfied:

$$\frac{N}{\varphi_x A} + \frac{\beta_{mx} M_x}{\gamma_x W_x (1 - 0.8(N/N'_{Ex}))} + \eta \frac{\beta_{ty} M_y}{\varphi_{by} W_y} \leq f \tag{8.6}$$

$$\frac{N}{\varphi_y A} + \eta \frac{\beta_{tx} M_x}{\varphi_{bx} W_x} + \frac{\beta_{my} M_y}{\gamma_y W_y (1 - 0.8(N/N'_{Ey}))} \leq f \tag{8.7}$$

where N is the design value of the compression force, M_x and M_y are the design moments about the major (x) and the minor (y) axes, respectively, φ_x and φ_y are the reduction factors for flexural buckling about the major (x) and the minor (y) axes, respectively, φ_{bx} is the reduction factor for lateral-torsional buckling,

Table 8.8 Calibration of ANSI/AISC 360-16 for Q690 steel welded H-sections under combined compression and bending.

Test	N_{test} (kN)	λ	$\overline{\lambda}$	ANSI/AISC 360-16	
				$P_{r,ANSI}$ (kN)	$N_{test}/P_{r,ANSI}$
EH1P	328	66	1.26	335	0.98
EH1Q	250	92	1.77	256	0.98
EH2P	527	53	1.01	515	1.02
EH2Q	418	74	1.42	426	0.98
EH3P	1698	39	0.77	1713	0.99
EH3Q	1376	55	1.08	1409	0.98
EH4P	2662	32	0.62	2449	1.09
EH4Q	2276	44	0.87	2182	1.04
Average	–	–	–	–	1.01

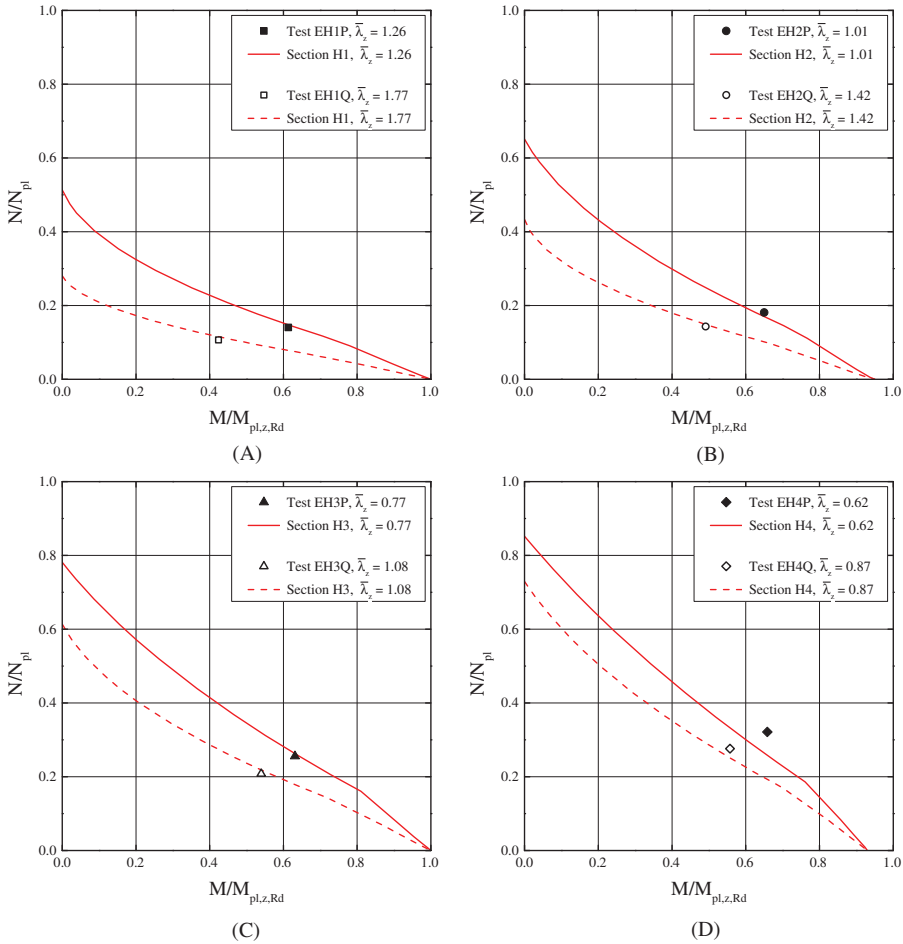

Figure 8.10 Normalized interaction curves to ANSI/AISC 360-16: (A) Section H1, (B) Section H2, (C) Section H3, and (D) Section H4.

$\varphi_{by} = 1.0$, $N'_{Ex} = \pi^2 EA/\left(1.1\lambda_x^2\right)$, $N'_{Ey} = \pi^2 EA/\left(1.1\lambda_y^2\right)$, λ_x, λ_y are the slendernesses for flexural buckling about the major (x) and the minor (y) axes, respectively, A is the cross sectional area, W_x and W_y are the elastic moduli about the major (x) and the minor (y) axes, respectively, β_{mx} and β_{my} are equivalent uniform in-plane moment factors about the major (x) and the minor (y) axes, respectively, β_{tx} and β_{ty} are equivalent uniform out-of-plane moment factors about the major (x) and the minor (y) axes, respectively, γ_x and γ_y are factors considering material plasticity when bending about the major (x) and the minor (y) axes, respectively, $\eta = 1.0$ for members susceptible to torsional deformation, $\eta = 0.7$ for members not susceptible to torsional deformation, f design yield strength of the steel material, and E is Young's modulus of the steel material.

A curve "b" is recommended to calculate flexural resistances of welded H-sections made of Q420 steel, the highest steel grade incorporated in GB50017-2003. The corresponding design resistances $N_{GB,b}$ are adopted for calibration against the test results. In addition, a curve "a" is also permitted in the code, and the corresponding design resistances $N_{GB,a}$ are also adopted for calibration. It should be noted that both the design resistances $N_{GB,a}$ and $N_{GB,b}$ are obtained through iterations. Comparison between the failure loads and the design resistances are shown in Table 8.9, while normalized interaction curves are plotted in Fig. 8.11. It is found that the test results are significantly higher than the design resistances obtained with either curve "b" or curve "a."

8.2.2 Box sections

8.2.2.1 Material properties

The Q460C steel used in this study is high-strength low alloy structural steel with the nominal yield strength of 460 MPa in GB/T 1591-2008 [4]. The nearest equivalent steel of Q460C according to EN 10025-6 [5] is S460N but the latter requires an additional verification of impact energy at −20°C. Tensile coupon tests were carried out to measure the mechanical properties of Q460C steel. A total of nine coupons were cut from the 11 mm parent plates. The cutting direction was perpendicular to the rolling direction according to GB/T 2975-1998 [6]. The tensile coupons were tested in accordance with GB/T 228-2002 [7]. Fig. 8.12 shows that, unlike normal-strength steel, no significant strain hardening appears in HSS Q460C steel. For some tensile coupons, there is no well-defined yield plateau. The average values of the test results are summarized in Fig. 8.12, where f_y is the 0.2% proof stress, which is adopted as the yield strength of Q460C steel, f_u is the ultimate tensile stress, E is Young's modulus, and Δ is the percentage of elongation after fracture.

Table 8.9 Calibration of GB 50017-2003 for Q690 steel welded H-sections under combined compression and bending.

Test	N_{test} (kN)	λ	$\overline{\lambda}$	GB 50017-2003			
				$N_{GB,b}$ (kN)	$N_{test}/N_{GB,b}$	$N_{GB,a}$ (kN)	$N_{test}/N_{GB,a}$
EH1P	328	66	1.26	268	1.23	275	1.19
EH1Q	250	92	1.77	218	1.15	223	1.12
EH2P	527	53	1.01	425	1.24	437	1.21
EH2Q	418	74	1.42	361	1.16	371	1.13
EH3P	1698	39	0.77	1380	1.23	1419	1.20
EH3Q	1376	55	1.08	1149	1.20	1191	1.16
EH4P	2662	32	0.62	2062	1.29	2110	1.26
EH4Q	2276	44	0.87	1860	1.22	1930	1.18
Average	–	–	–	–	1.21	–	1.18

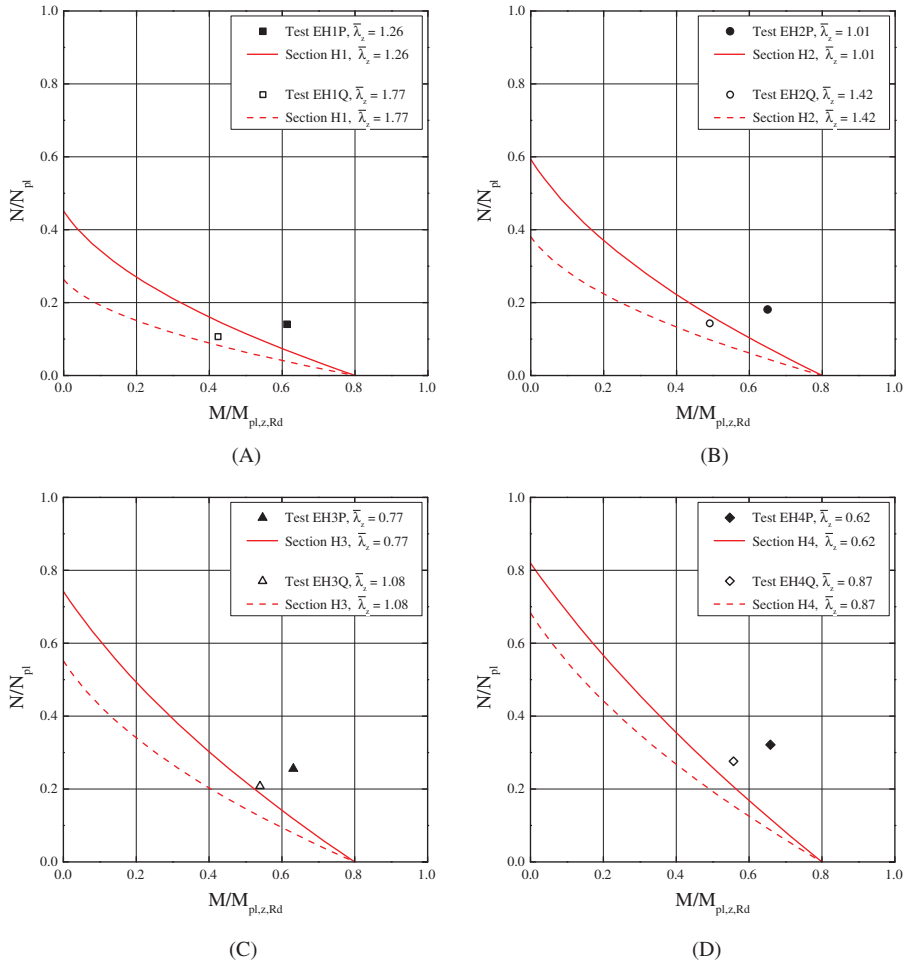

Figure 8.11 Normalized interaction curves to GB 50017-2003: (A) Section H1, (B) Section H2, (C) Section H3, and (D) Section H4.

8.2.2.2 Specimen design and fabrication

To evaluate the behavior of Q460C box columns under eccentric compression, seven specimens with sectional width to thickness ratios from 7.6 to 17.5 were fabricated from flame-cut Q460C steel plate. Four 11 mm component plates were welded together to form a box-section specimen by manual GMAW, as shown in Fig. 8.13. The electrode ER55-D2 was used to achieve equivalent-matching weld with Q460C steel. As current practice does not employ complete penetration welding for columns except in the beam-to-column connection zone, the component plates were connected by incomplete penetration welding except the 500 mm length from each end. In order to reduce the effect of shrinkage deformation caused by

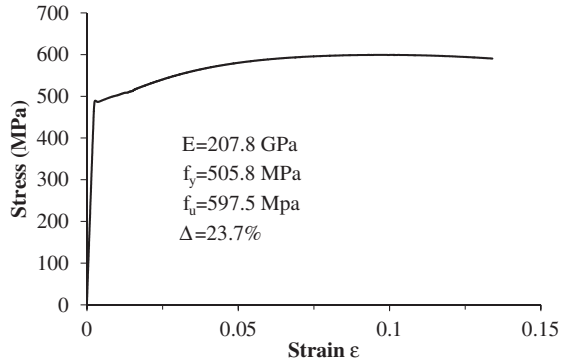

Figure 8.12 Stress−strain relationship of Q460C steel.

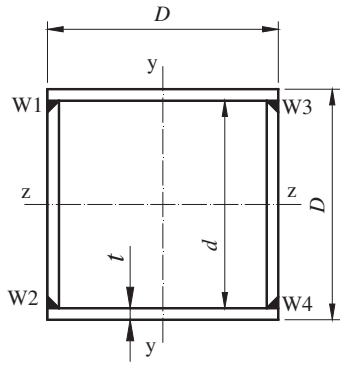

Figure 8.13 Definition of symbols.

welding heating and cooling, the optimized welding sequence (W1→W2→W3→W4) was adopted, as shown in Fig. 8.13. The measured geometric dimensions of the seven test specimens are shown in Table 8.10. The specimens were named in terms of B-d/t-λ-X-n, where B is for box-section and n is the specimen number. The tests were designed to investigate the overall buckling behavior of the welded HSS box columns under eccentric load. Thus premature local buckling is prevented by limiting the plate slenderness ratio.

In the Chinese Code for design of steel structures GB 50017-2003 [8]:

$$d/t \le (25 + 0.5\lambda)\sqrt{\frac{235}{f_y}}, \quad 30 \le \lambda \le 100 \tag{8.8}$$

The plate slenderness limits are ranging from 28.6 to 53.6 depending on the λ varying from 30 to 100.

In the European code for design of steel structures Eurocode 3 [9]:

$$d/t \leq 42\sqrt{\frac{235}{f_y}} \tag{8.9}$$

Thus the plate slenderness limit of Class 3 section is 30.0.

The d/t of 17.5 (section B-18) was selected to represent the commonly used aspect ratio for Q460C steel; the d/t of 11.5 (section B-12) was considered as the lower boundary of the columns fabricated from Q460C steel in industry practice; and the section B-8 with d/t of 7.7 was designed to investigate the extreme case. The plate slenderness ratios are all lower than the plate slenderness limits, specified either in the GB 50017-2003 or in the Eurocode 3. Thus premature local buckling is not expected to occur before the peak load, and the overall buckling will dominate the ultimate bearing capacities of the test columns.

8.2.2.3 Out-of-straightness and loading eccentricity

Initial geometric imperfection consists of initial out-of-straightness and initial loading eccentricity, as shown in Fig. 8.14. The initial out-of-straightness was unavoidably caused by the nonuniform weld shrinkage during the manufacture process. A prestressed string was attached tightly to the two ends of the component plate to provide a straight reference line, and the deviations at seven points with equal interval were measured. The measurement process was repeated after rotating the

Table 8.10 Measured dimensions of test specimens.

Specimen	D	t	d/t	L	L_e	A	I	r	λ
	mm	mm		mm	mm	mm^2	cm^4	mm	
B-8-80-X-1	110.0	11.5	7.6	3000	3320	4531	743	40.5	82.0
B-8-80-X-2	110.8	11.5	7.6	2940	3260	4581	767	40.9	79.6
B-8-80-X-3	112.5	11.3	8.0	3000	3320	4574	791	41.6	79.8
B-12-55-X-1	155.2	11.5	11.5	2940	3260	6610	2290	58.9	55.4
B-12-55-X-2	153.3	11.5	11.3	2940	3260	6523	2200	58.1	56.1
B-18-38-X-1	222.0	11.4	17.5	2940	3260	9603	7120	86.1	37.9
B-18-38-X-2	219.8	11.5	17.1	2940	3260	9582	6950	85.2	38.3

Note: L is the net length of the column not accounting end plates, L_e is the effective length of column between two pinned supports, A is the area of box-section, I is the moment of inertia of box-section, r is the gyration radius, and λ is the slenderness where $\lambda = L_e/r$.

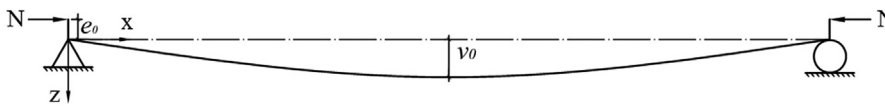

Figure 8.14 Geometric imperfections.

specimens by 90 degrees. To reduce measurement errors the average value of initial out-of-straightness v_0 obtained on both sides was adopted. The values of v_0 at mid-height cross section are summarized in Table 8.11. The test specimens were set under eccentric loading. The intentional loading eccentricity was introduced by the deviation between the central axis of column cross section and the central axis of end plate, as shown in Fig. 8.15. The measured loading eccentricities of both ends were averaged and summarized in Table 8.11.

8.2.2.4 Test setup and loading procedure

The specimens were tested under eccentric loading with a 10,000 kN universal testing machine at Tongji University. The schematic diagram of the test setup is shown in Fig. 8.16. Two curved surface supports were used at both ends of each specimen, which can be recognized as ideal hinged connection in the bending plane, while they are fixed about the other principal axis of the cross section. All specimens were set to pin-supported about the y−y axis and fixed the about z−z axis. The arrangement of the linear varying displacement transducers (LVDTs) and the strain gages is shown in Fig. 8.16. The axial deformation of the specimens was measured by the LVDTs V1 and V2. The LVDTs H01−H03 were placed at the midlength of the column to record the in-plane lateral deflections. The out-of-plane lateral

Table 8.11 Initial geometric imperfections.

Specimen	e_0 mm	v_0 mm
B-8-80-X-1	48.1	− 4.5
B-8-80-X-2	54.6	− 6.0
B-8-80-X-3	53.4	− 6.1
B-12-55-X-1	55.4	− 2.8
B-12-55-X-2	53.4	3.5
B-18-38-X-1	66.0	− 1.0
B-18-38-X-2	65.5	− 1.7

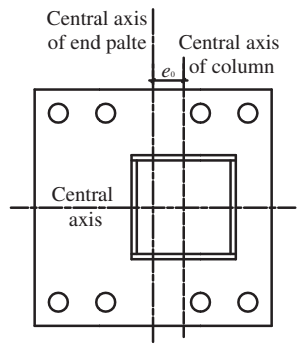

Figure 8.15 Loading eccentricity.

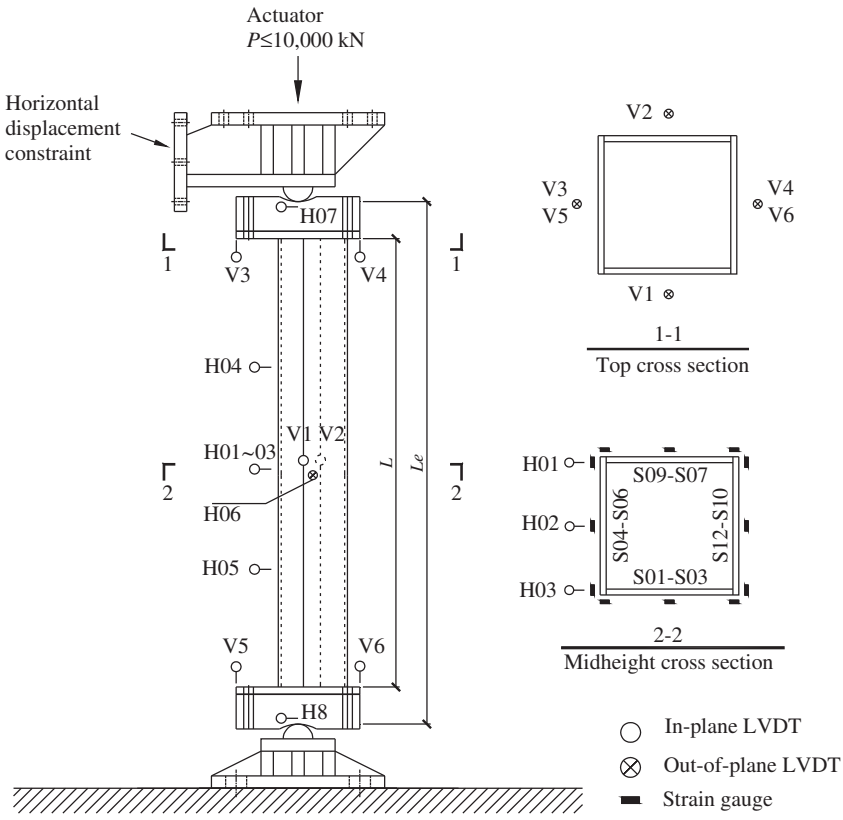

Figure 8.16 Test setup.

deflection was captured by the LVDT H06. The strain gages were attached to the midlength cross section of the specimens to monitor the loading force. The real-time load−deflection curves and load-shortening curves displayed in the monitor during the entire loading processes were used to adjust and govern the experiments.

Before the actual test a preload with 10% of the predicted maximum column strength was used to check the test instrumentations and then unloaded. In the actual test the axial load was applied on the column at a rate of 1 mm/min until the peak load was reached. Then the load rate was increased in the postpeak range. Finally, the test specimen was unloaded to finish the test procedure when the test load decreased to 80% of the peak load.

8.2.2.5 Assessment of test result

Overall buckling behavior

The measured axial load versus midheight deflection curves are shown in Fig. 8.17. The average deflection of H01−H03 is used, since the readings obtained from

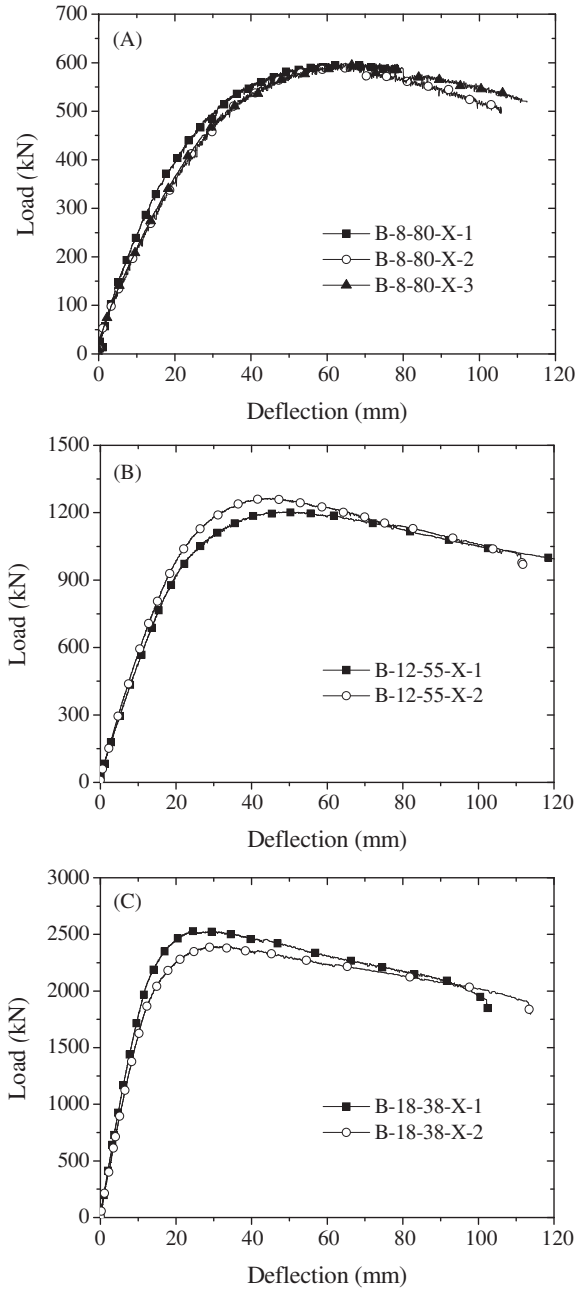

Figure 8.17 Load−defection curves: (A) B-8-80 series, (B) B-12-55 series, and (C) B-18-38 series.

H01−H03 differs slightly from each other. The specimens show a stable load−deflection relationship, including initial elastic loading branch, inelastic hardening branch, and gradual softening branch, which indicates a ductile behavior under large deformation. The measured out-of-plane lateral deflection is so small that can be ignored. The observed failure mode of the specimens, with various member slenderness ratios of 38−80, is identified as flexural buckling in the intended direction, as shown in Fig. 8.18. Local buckling was not observed before peak load. For the specimens B-18-38-X-1 and B-18-38-X-2, local buckling was observed at midheight cross section just before the load dropping to 80% of the maximum load. The measured ultimate loads P_u of the specimens subjected to eccentric loading are summarized in Table 8.12.

The typical axial load−strain curves measured at the midheight cross section are shown in Fig. 8.19. As shown in Fig. 8.16, the strain gages S05 and S11 were

Figure 8.18 Initial loaded specimens and specimens near failure: (A) B-8-80-X-1, (B) B-12-55-X-1, and (C) B-18-38-X-1.

Table 8.12 Comparison of experimental and predicted ultimate resistances.

Specimen	P_u (kN)	P_u/Af_y	GB 50017 N_{GB} (kN)	GB 50017 N_{GB}/P_u	Eurocode 3 N_{EC3} (kN)	Eurocode 3 N_{EC3}/P_u
B-8-80-X-1	598.5	0.261	448.6	0.75	509.8	0.85
B-8-80-X-2	598.0	0.258	443.1	0.74	487.3	0.81
B-8-80-X-3	599.0	0.259	451.3	0.75	532.4	0.89
B-12-55-X-1	1204.5	0.360	967.2	0.80	1041.7	0.86
B-12-55-X-2	1264.5	0.383	954.7	0.76	1098.1	0.87
B-18-38-X-1	2532.0	0.521	1846.8	0.73	1417.5	0.56
B-18-38-X-2	2394.0	0.494	1821.3	0.76	1363.4	0.57
		Mean value		0.76		0.77
		Standard deviation		0.02		0.14

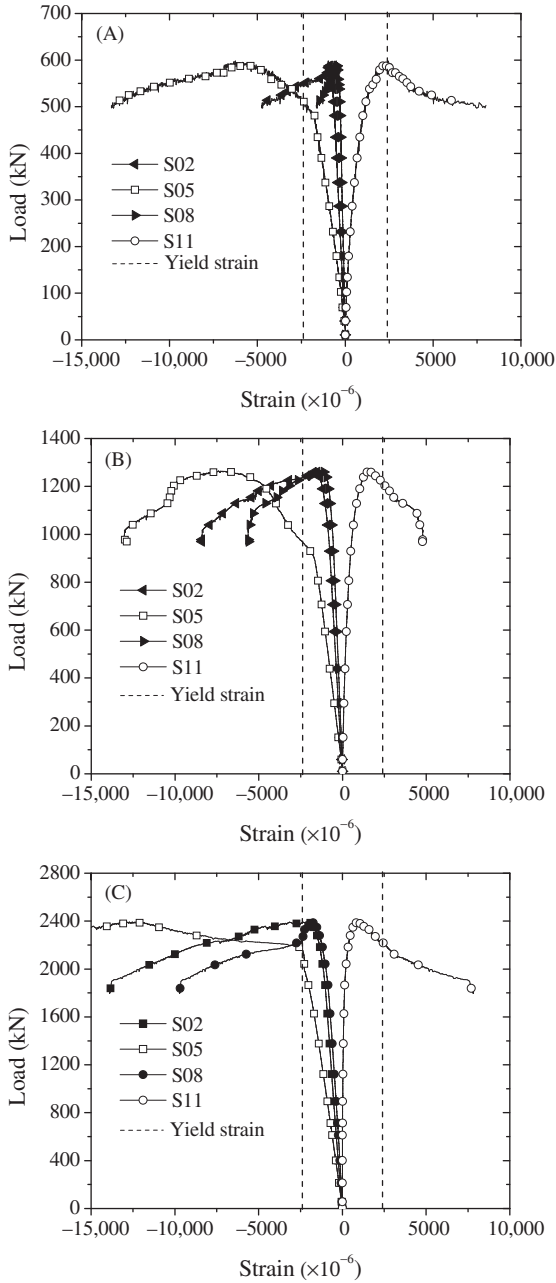

Figure 8.19 Load−strain curves: (A) B-8-80-X-2, (B) B-12-55-X-2, and (C) B-18-38-X-2.

attached on the midwidth of right and left flanges of the box-section, respectively. The strain gages S02 and S08 were attached on the middepth of webs. Consequently, the bending effect can be identified from the difference of the axial strain between the component plates. Fig. 8.19 shows that, due to the preset eccentricity, the midheight cross section is subjected to compression and bending at the beginning of loading. Thus the specimens show a limit load instability instead of bifurcation buckling of concentrically loaded columns. With the increase in test load the second-order effect becomes obvious, and the difference of axial strain between the extreme compressive and tensile fibers becomes remarkable. The extreme compressive fibers (S05) yields before peak load for all specimens, while the strains of extreme tensile fibers (S11) are lower than yield strain (f_y/E) before peak load. However, it should be noted that RS induced by welding process could advance or postpone yielding of steel, depending on the superimposed compressive or tensile RS. The strain of middle fibers such as that recorded by strain gages S02 and S08, which can be recognized as the average strain of the cross section, reveals the stress ratio of the cross sectional resistances. At peak load the middle fiber strains of the specimens with column slenderness ratio of 80, 55, and 38 are 63%, 88%, and 92% of f_y/E, respectively. Similar as buckling factor, the middle fiber strain to f_y/E ratio increases with the decrease in column slenderness ratio.

Comparison of test results with design codes

Slender steel members subjected to combined bending and axial compression are generally limited by buckling resistance. Thus in addition to cross section resistance, the beam−column member should be verified against buckling interaction formula. In the case of uniaxial eccentric loading, the buckling interaction formulae can be reduced as follows:

$$\text{According to GB50017-2003}\ \frac{N}{\chi_y A}+\frac{\beta_{my}M_y}{\gamma_y W_{1y}(1-\eta_1(N/N'_{Ey}))}\le f_y \tag{8.10}$$

$$\text{According to Eurocode 3}\ \frac{N}{\chi_y N_{Rk}/\gamma_{M1}}+k_{yy}\frac{M_y+\Delta M_y}{\chi_{LT}\left(M_{y,Rk}/\gamma_{M1}\right)}\le 1 \tag{8.11}$$

where N and M_y are the design values of the compression force and the maximum moments about the y−y axis along the column, ΔM_y is the moment due to the shift of the centroidal axis for Class 4 sections, N_{Rk} and $M_{y,Rk}$ are the characteristic compressive resistance and characteristic moment resistance about y−y axis of the cross section, χ_y is the reduction factor due to flexural buckling, β_{my} is the equivalent coefficient of moment distribution, W_{1x} is the elastic section modulus, k_{yy} is the interaction factor, $\gamma_{M1}=1.00$, γ_y is inelastic development factor and $\gamma_y=1.05$, η_1 is the compensation coefficient with $\eta_1=0.8$ for normal-strength steel, and $N'_{Ey}=\pi^2EA/(1.1\lambda^2)$. According to both GB 50017-2003 and Eurocode 3, the buckling curve "c" is the design curve for the tested box-section with d/t ratio less than

20 and ΔM_y is zero. Considering box-section member with twisting restrained supports at both ends, it is not susceptible to lateral-torsional buckling. Thus the reduction factor $\chi_{LT} = 1$ was adopted in the calculation.

Table 8.12 compares the design strengths of GB 50017-2003 and Eurocode 3 with the test strengths. All test results are higher than the predicted value, indicating the conservative of the current design formulae. The ultimate load bearing capacity of the tested Q460C box-section columns is underestimated by 24% and 23% in accordance with GB 50017-2003 and Eurocode 3, respectively. The similar underestimation has been found in the concentrically loaded Q460C HSS box columns [10], however, which is less pronounced than that of eccentrically loaded Q460C HSS box columns. The main reason for the underestimation of ultimate resistance is recognized as the less detrimental effect of imperfections on HSS members, such as RS and initial out-of-straightness caused by welding process, than those on normal-strength steel columns. Moreover, the compressive RS to the yield strength ratios of Q460C HSS box-sections are lower than those adopted for normal-strength steel in the current codes [11]. It is noted that Eurocode 3 can give better perdition than GB 50017-2003 for columns with high slenderness. However, for columns with medium slenderness, Eurocode 3 gives more conservative results than GB 50017-2003 by up to 44%.

8.3 Numerical investigation

In this numerical investigation, validated numerical models were initially developed through accurate replication of the test results. Parametric studies were performed subsequently to examine further the influences of member residual stresses and material tensile to yield strength ratios on the structural response of HSS columns of welded sections under combined compression and bending.

8.3.1 H-sections

Having validated the numerical models against the experimental results [3], a series of parametric studies was performed, focusing on residual stresses and material tensile to yield strength ratios. The measured residual stress ratios of Q690 steel columns of welded H-sections were found to be significantly smaller than the assumed values by ECCS for conventional steel columns of welded H-sections, and thus the adverse effect from residual stresses on Q690 steel columns of welded H-sections was anticipated to be less than that on conventional steel columns of welded H-sections. The degree of residual stress effect for Q690 steel and Q235 steel columns of welded H-sections will be compared in the following studies. Another factor that may affect the buckling resistances of Q690 welded H-sections is material tensile to yield strength ratios. The tensile to yield strength ratios indicate the abilities of strain hardening of the materials. For conventional steel material, strain hardening develops at the end of a long yield plateau. In the simulation of conventional steel

members the resistance of which is dominated by instability, an elastic-perfectly plastic model is practically adopted, and the strain hardening is neglected. However, for Q690 steel, the strain hardening starts once the material is yielding. Therefore for Q690 steel columns of welded H-sections, the neglection of strain hardening may lead to a conservative design. The contribution of strain hardening to the buckling resistances is related to the tensile to yield strength ratios. In the following studies the effect of tensile to yield strength ratios is evaluated for Q690 steel columns of welded H-sections under combined compression and bending.

In the generation of FE models, all the steel columns were modeled by using shell elements S4R. Section H3 was selected as a typical cross section size. The nondimensional slendernesses of these FE models ranged from 0.6 to 1.8 with an interval of 0.4. To normalize the initial loading eccentricity with the cross-sectional properties, an initial loading eccentricity ratio is defined by Eq. (8.12), where e is the initial loading eccentricity, A is the area of cross section, and W_{el} is the elastic modulus of cross section. For each nondimensional slenderness the initial loading eccentricity ratios varied from 0.0 (compression only) to 20.0 (combined compression and bending):

$$\varepsilon = \frac{eA}{W_{el}} \tag{8.12}$$

The shape of the initial out-of-straightness was assumed to be a sinusoidal shape, and the amplitude was replaced by $L_{eff}/1000$. The initial out-of-straightness and the initial loading eccentricity were positioned on different sides of the longitudinal axis of the welded H-sections.

8.3.1.1 Residual stresses

To evaluate the effect of residual stresses on Q690 steel columns of welded H-sections, buckling resistances were obtained from two groups of FE models, in which one with residual stresses and the other one without residual stresses. The residual stress amplitudes for Q690 steel welded H-section H3 were shown in Table 8.13.

Table 8.13 FE model information for the evaluation of effect of residual stresses.

Group	Bending axis	Steel grade	Residual stresses	Initial out-of-straightness v	Model numbers	Nondimensional Slenderness
1	Major	690	No	$L_{eff}/1000$	60	0.6/1.0
2			Yes		60	1.4/1.8
3		235	No		60	
4			Yes		60	
5	Minor	690	No		60	
6			Yes		60	
7		235	No		60	
8			Yes		60	

A total of 240 numerical models were established, and their information is summarized in Table 8.13. In this study the overall flexural buckling was not restricted in minor axis but extended to major axis. The material behavior of Q690 steel was modeled as an elastic-linear hardening relationship, as shown in Fig. 8.20. The mechanical properties of Q690 steel were obtained in standard the tensile tests, and the key parameters in true stress−logarithmic plastic strain behavior are shown in Fig. 8.20.

To compare the effect of residual stresses on Q690 steel columns of welded H-sections with that on Q235 steel columns, FE models with Q235 steel were generated, and their model information is also summarized in Table 8.13. The residual stress pattern for Q235 steel columns of welded H-sections is shown in Table 8.14. The material behavior of Q235 steel was modeled as a multilinear relationship, as shown in Fig. 8.20. The yield strength was taken to be its nominal value, 235 MPa, and the tensile strength was 370 MPa according to GB/T 700 and EN 10025-2 [5]. The $\varepsilon_{st,log}$ and $\varepsilon_{u,log}$ are the strain at the end of yield plateau and the ultimate strain, respectively. The key parameters in true stress−logarithmic plastic strain behavior are shown in Table 8.14.

Figs. 8.21 and 8.22 depict the normalized compression and bending relationships of FE models, arranged by nondimensional slenderness, $\overline{\lambda}$. In these figures, N_{FEM} is the buckling resistance obtained from the finite element models, $M_{FEM} = N_{FEM}ee$,

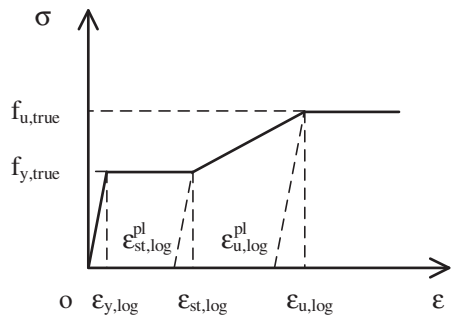

Figure 8.20 True stress−logarithmic strain relationships for Q235 steel plates.

Table 8.14 True stress−logarithmic plastic strain relationship for Q235 steel plates in FE models.

Young's Modulus E (kN/mm^2)	True yield strength $f_{y,true}$ (N/mm^2)	True strength onset of strain hardening $f_{st,true}$ (N/mm^2)	logarithmic plastic strain onset of strain hardening $\varepsilon^{pl}_{st,log}$	True tensile strength $f_{u,true}$ (N/mm^2)	Logarithmic plastic ultimate strain $\varepsilon^{pl}_{u,log}$
210	235	240	0.024	444	0.182

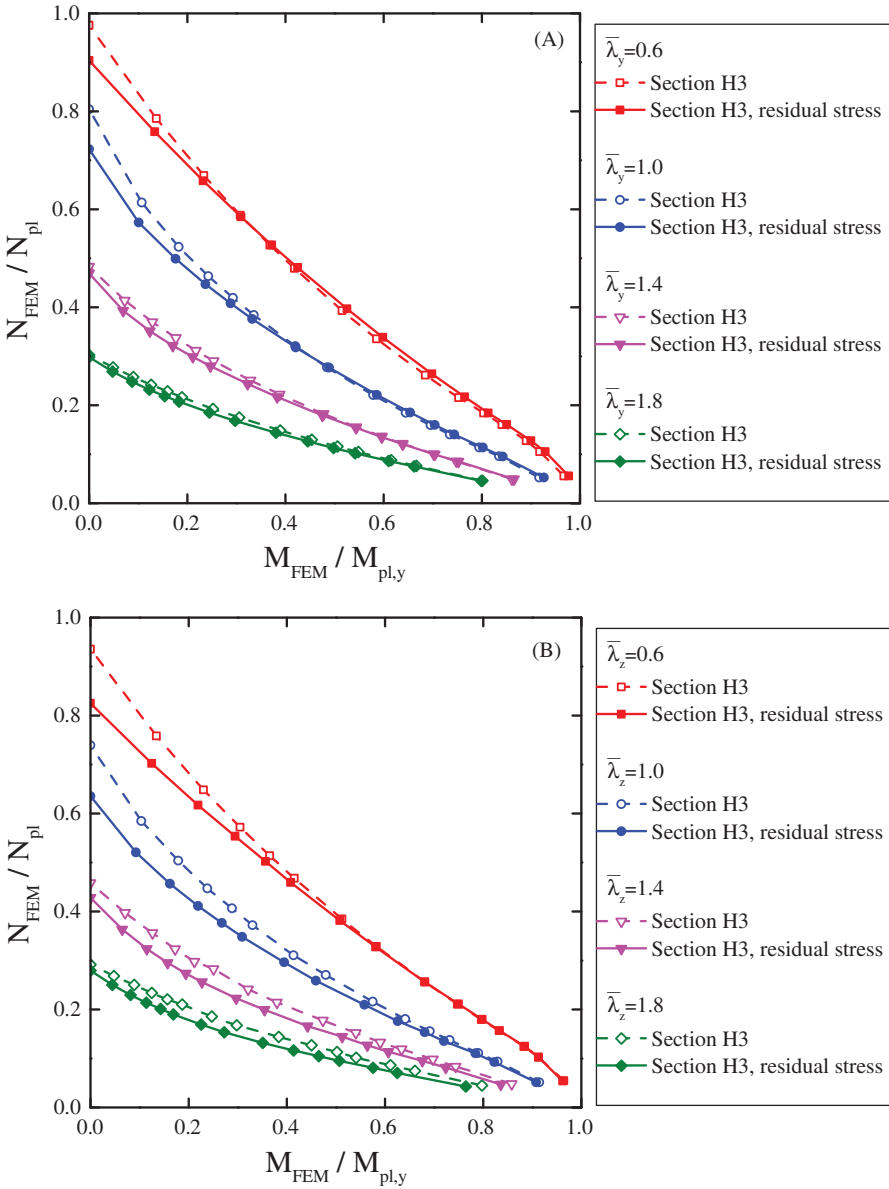

Figure 8.21 Effect of residual stresses on buckling resistances of Q690 and Q235 steel columns of welded H-sections under combined compression and major axis bending: (A) Q690 steel columns of welded H-sections and (B) Q235 steel columns of welded H-sections.

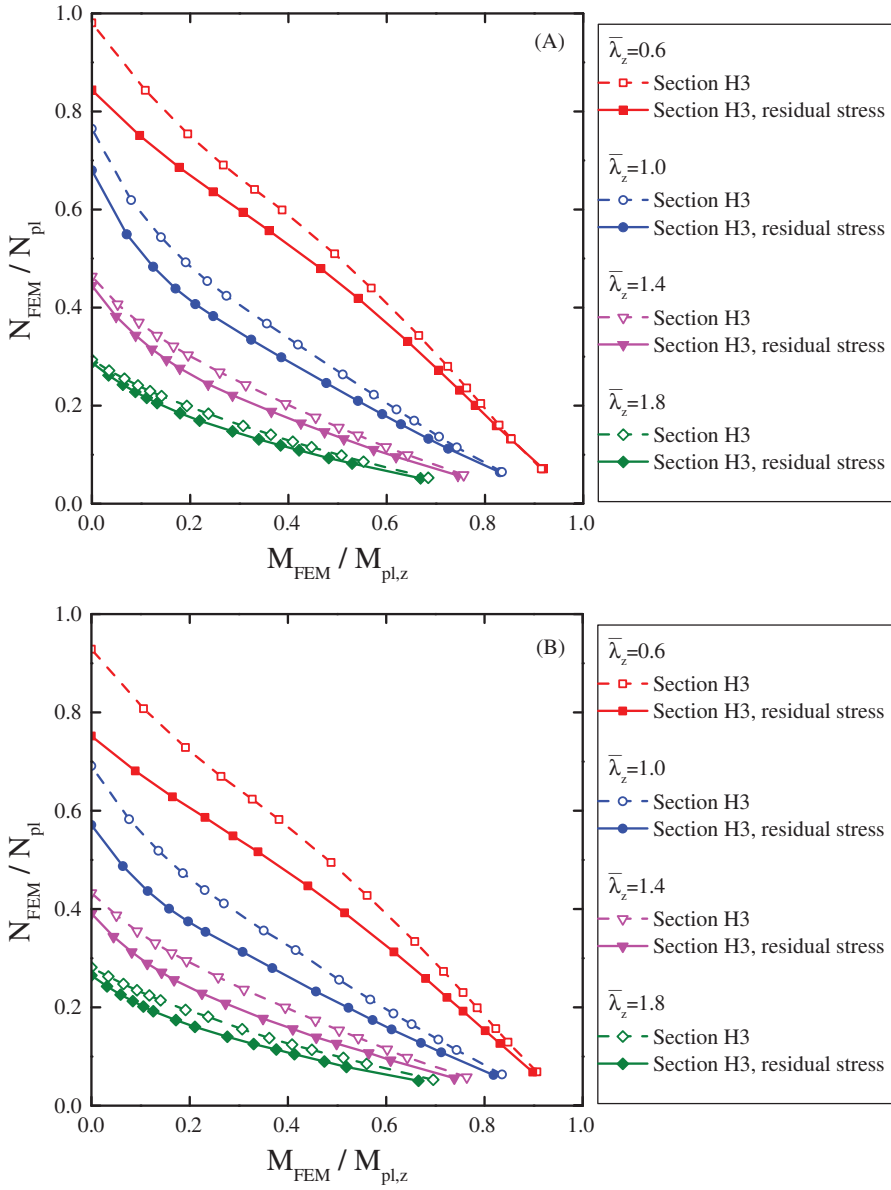

Figure 8.22 Effect of residual stresses on buckling resistances of Q690 and Q235 steel columns of welded H-sections under combined compression and minor axis bending: (A) Q690 steel columns of welded H-sections and (B) Q235 steel columns of welded H-sections.

$N_{pl} = Aef_y$, and M_{pl} is the sectional plastic resistance to bending moment. It is found that:

1. The presence of residual stresses reduces the buckling resistances of both Q690 and Q235 steel columns of welded H-sections under combined compression and bending. Compared with Q235 steel columns of welded H-sections, the effect degree becomes less on Q690 steel columns of welded H-sections with the same nondimensional slenderness and initial loading eccentricity ratio.
2. For both Q690 and Q235 steel columns of welded H-sections, when the nondimensional slendernesses of the columns are 0.6 and 1.0, the effect of residual stresses decreases with the increase of initial loading eccentricity ratio. However, when the nondimensional slendernesses of the columns are 1.4 and 1.8, the effect of residual stresses initially increases and subsequently decreases with the increase of initial loading eccentricity ratio.

Overall, residual stresses can significantly reduce the buckling resistances of Q690 steel columns of welded H-sections under combined compression and bending. But compared with Q235 steel columns of welded H-sections, the effect of residual stresses is decreased for Q690 steel columns of welded H-sections due to the smaller ratios of residual stresses to yield strength.

8.3.1.2 Tensile to yield strength ratios

To evaluate the effect of tensile to yield strength ratios on Q690 steel columns of welded H-sections, buckling resistances were obtained from FE models with two different material stress−strain models, (1) an elastic-linear hardening model (see Fig. 8.23) and (2) an elastic-ideally plastic model, as shown in Fig. 8.23. The mechanical properties of these two models are listed in Table 8.15, and only E and $f_{y,true}$ were included in the elastic-ideally plastic model. A total of 240 numerical models were established, and their information are summarized in Table 8.15. The residual stress pattern for Q690 steel welded H-section H3 is listed in Table 8.15. The overall flexural buckling was not restricted in minor axis but extended to major axis.

To compare the effect of tensile to yield strength ratios on Q690 steel columns of welded H-sections with that on Q235 steel columns of welded H-sections, FE models with Q235 steel were generated, and their model information is also

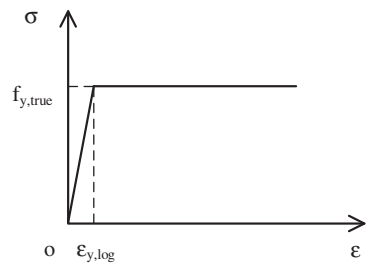

Figure 8.23 Elastic-ideally plastic model.

Table 8.15 FE model information for the evaluation of the effect of tensile to yield strength ratios.

Group	Bending axis	Steel grade	f_u/f_y	Residual stresses	Initial out-of-straightness v	Model numbers	Nondimensional slenderness
1	Major	690	1.00	Yes	$L_{eff}/1000$	60	0.6/1.0
2			1.05			60	1.4/1.8
3		235	1.00			60	
4			1.57			60	
5	Minor	690	1.00			60	
6			1.05			60	
7		235	1.00			60	
8			1.57			60	

summarized in Table 8.15. Two different material stress−strain models were considered, (1) a multilinear model (see Fig. 8.20) and (2) an elastic-ideally plastic model (see Fig. 8.23). The mechanical properties of these two models are listed in Table 8.14, and only E and $f_{y,true}$ were excluded in the elastic-ideally plastic model. A total of 240 numerical models were established, and their information is summarized in Table 8.15. The overall flexural buckling was not restricted in minor axis but extended to major axis.

Figs. 8.24 and 8.25 depict the normalized compression and bending relationships of FE models, arranged by nondimensional slenderness, $\overline{\lambda}$. It is found that:

1. For Q235 steel columns of welded H-sections, even though the strain hardening is considered in the stress−strain model, there is no increase in the buckling resistances of the models. This has been commonplace and lies in the fact that there is a long yield plateau in the stress−strain relationship of Q235 steel, and when the H-sections fail, significant strain hardening does not take place.
2. For Q690 steel columns of welded H-sections, when considering strain hardening, some increases in the buckling resistances of the models are visible only in columns with nondimensional slenderness of 0.6. Because when a relatively short column fails, the strain is able to develop well beyond the yield strain, and thus the buckling resistance can take advantage of strain hardening. While when a long column fails, the strain is not able to develop beyond the yield strain, and the strain hardening cannot be mobilized.
3. The maximum increase in buckling resistance improved by strain hardening is only 2.0%, thus the elastic-ideally plastic model can be used in the modeling of buckling resistances of Q690 steel columns of welded H-sections under combined compression and bending without causing too much conservatism.

Overall, strain hardening can slightly improve the buckling resistances of Q690 steel short columns of welded H-sections, and the neglection of strain hardening will not result in a conservative design.

From the parametric studies earlier, it is concluded that the residual stresses can significantly affect the buckling resistances of Q690 steel columns of welded H-sections under combined compression and bending. Compared with the conventional steel

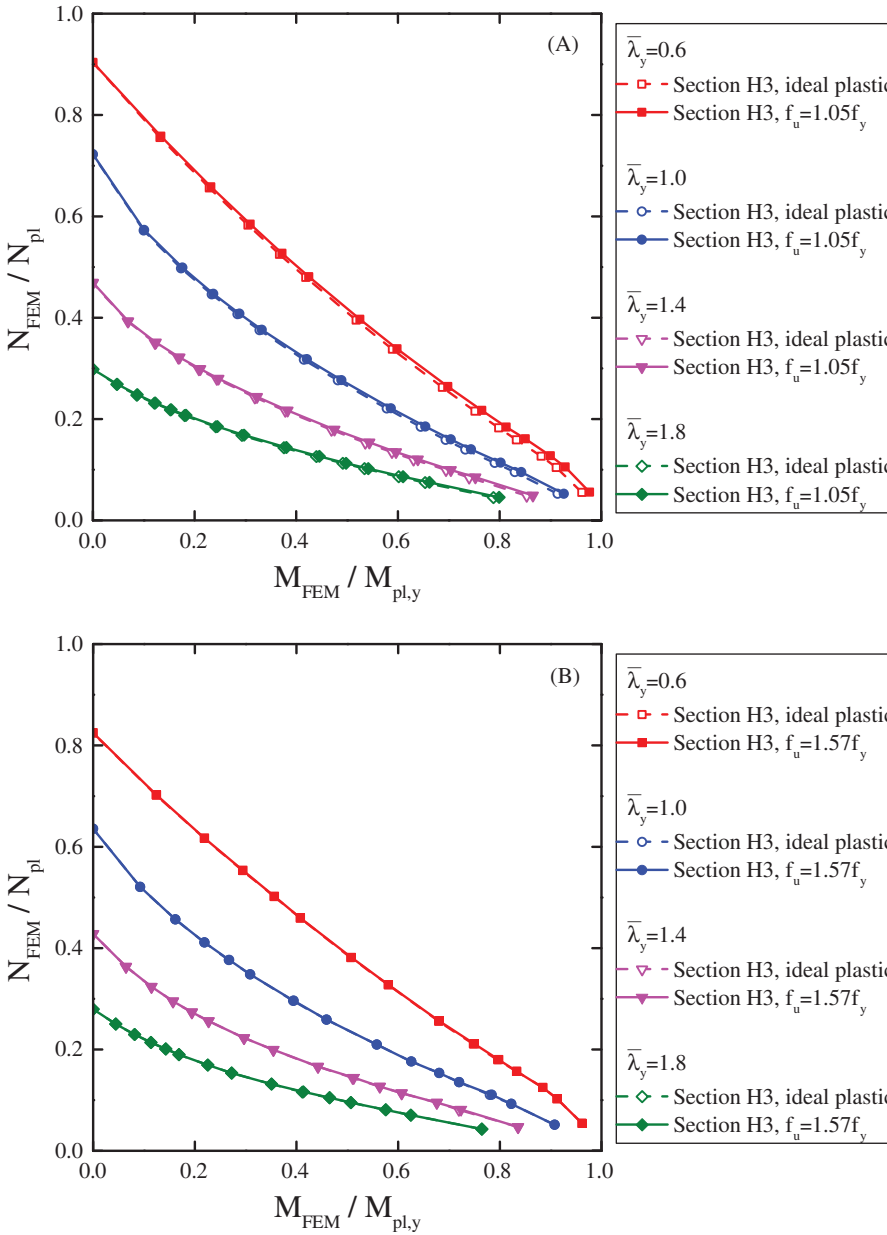

Figure 8.24 Effect of tensile to yield strength ratios on buckling resistances of Q690 and Q235 steel columns of welded H-sections under combined compression and major axis bending: (A) Q690 steel columns of welded H-sections and (B) Q235 steel columns of welded H-sections.

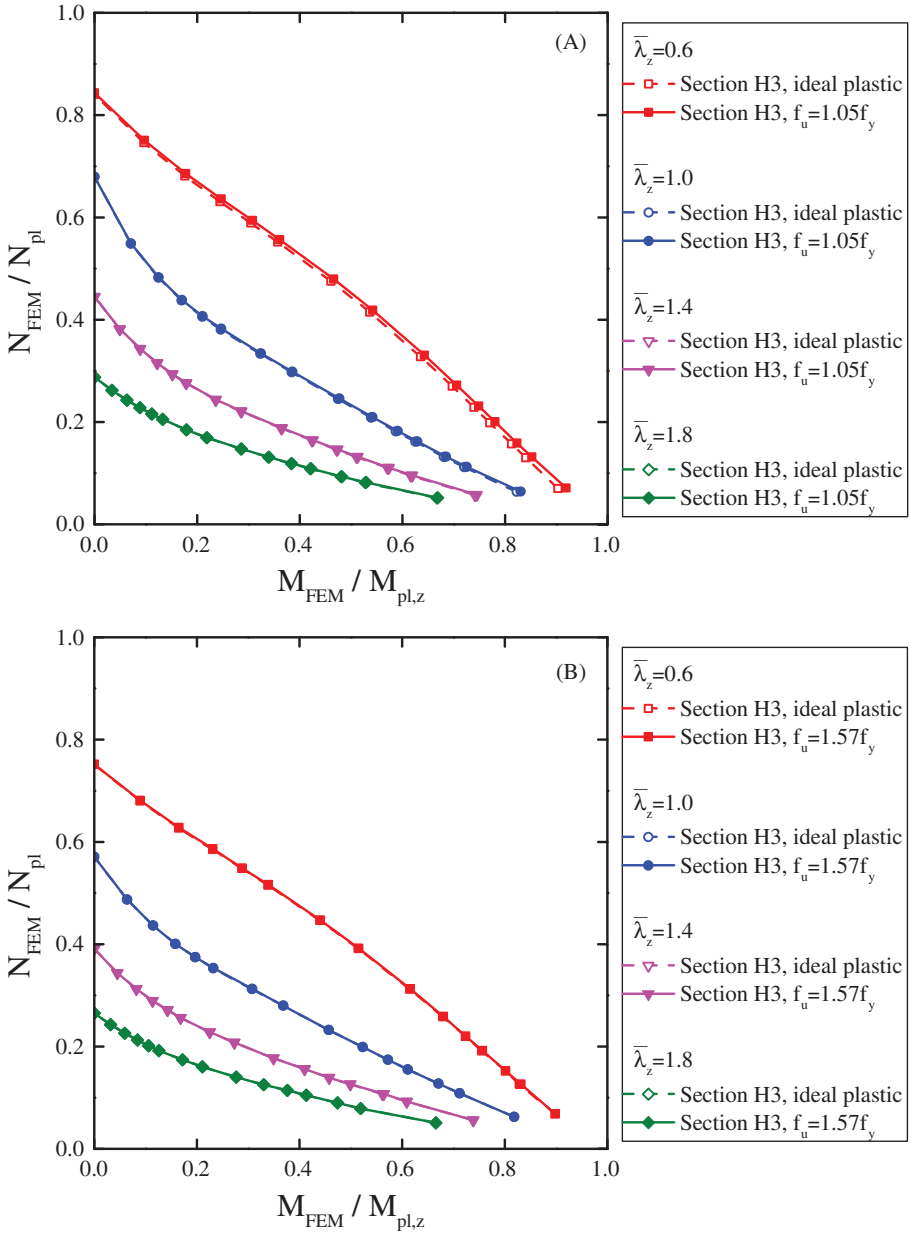

Figure 8.25 Effect of tensile to yield strength ratios on buckling resistances of Q690 and Q235 steel columns of welded H-sections under combined compression and minor axis bending: (a) Q690 steel columns of welded H-sections and (b) Q235 steel columns of welded H-sections.

materials, the effect of residual stresses becomes less pronounced in Q690 steel columns of welded H-sections. It should be noted that strain hardening barely contributes to the buckling resistances of the Q690 steel columns of welded H-sections.

8.3.2 Box sections

Since the finite element model can successfully predict the ultimate strength and the load−deflection behavior of the columns, the developed FE model is used to generate more data rather than the limited test results. The main parameters are width to thickness ratio (d/t in Table 8.16), column slenderness λ (from 10 to 160) and eccentricity ratio, $\varepsilon_0 = e_0A/W_{1y}$ (from 0 to 20 along y−y and z−z axes, respectively). The varying of RS is implicitly involved in the adoption of different cross sections with varying width to thickness ratios. The cross section dimensions and material properties are summarized in Table 8.16. A total of 2016 pin−pin columns with consideration of simplified RS pattern and $1000/L_e$ initial bow were analyzed. The results show that columns with eccentricity caused bending about y−y axis achieve slight lower ultimate strength than those bending about z−z axis. Thus on the conservative side, the following discussion is based on the eccentricity settled along z−z axis.

8.3.2.1 Effect of slenderness

To evaluate the effect of the slenderness on the behavior of eccentrically loaded columns, the calculated interaction curves of B-15 series with varying column slenderness are shown in Fig. 8.26. It can be observed that, with lower slenderness, the columns achieve higher buckling interaction curves. From the comparison of the predicted results with those without consideration of RS, the influence of RS on the interaction curves is revealed. Stocky columns with slenderness no more than 20 trend to be strength failure. Since RS does not impair cross-sectional strength, the interaction curves with and without consideration of RS almost coincide with each other (less than 1%). With increased slenderness higher than 20, columns are susceptible to overall buckling. The presence of compressive RS in compression side of midheight cross section will bring forward the yielding and reduce the moment of inertia. Consequently, for columns with mediate slenderness, the interaction curves with consideration of RS are lower than those ignored RS.

Table 8.16 Dimensions and material properties of specimens for parametric study.

Section	D (mm)	t (mm)	d	d/t	A (mm^2)	E (GPa)	f_y (MPa)
B-8	105.6	11	83.6	7.6	4162.4	207.8	505.8
B-10	127.6		105.6	9.6	5130.4		
B-12	148.5		126.5	11.5	6050.0		
B-15	187.0		165.0	15.0	7744.0		
B-18	211.2		189.2	17.2	8808.8		
B-20	242.0		220.0	20.0	10164.0		

For very slender column with slenderness over 120, it tends to buckle elastically. Thus the influence of RS on the ultimate strength of column is reduced.

8.3.2.2 Effect of eccentricity ratio

In order to evaluate the influence of eccentricity ratio, the deviations between predictions with and without consideration of RS (N_{RS} and N_0) are plotted against ε_0 in Fig. 8.27, where the deviation is defined as:

$$\Delta N = \frac{N_{RS} - N_0}{N_0} \times 100\% \tag{8.13}$$

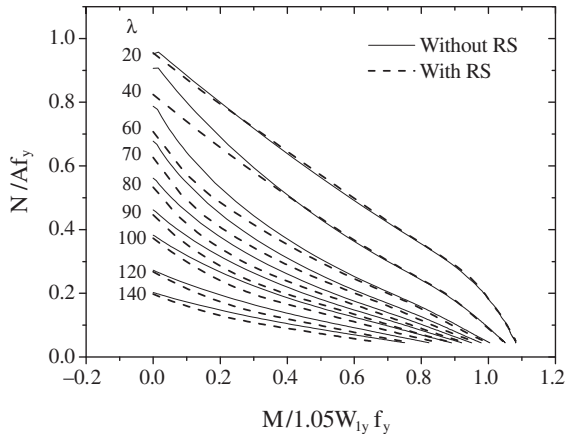

Figure 8.26 Interaction curves of the B-15 series with varying column slenderness.

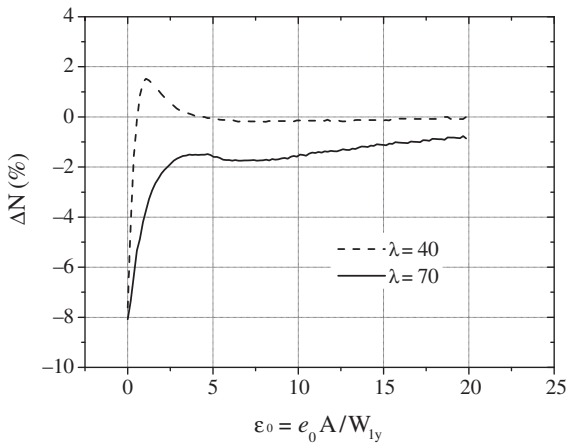

Figure 8.27 Effect of eccentricity ratio, B-15 series.

Because the ultimate strength of stub column and very slender column is less sensitive to RS, only $\Delta N - \varepsilon_0$ curves of mediate ($\lambda = 40$) and slender ($\lambda = 70$) columns of B-15 series are shown. According to Fig. 8.27, the influence of RS is significant with eccentricity ratio about no more than 5. With the increase in load eccentricity, the moment resistance of cross section becomes more importance than the buckling resistance of columns in compression. Thus the detrimental effect of RS decreases to less 2% with eccentricity ratio more than 5.

One the other hand, the two $\Delta N - \varepsilon_0$ curves with slenderness of 40 and 70 perform differently in detail with ε_0 ranging from 0 to 5. There is even positive effect of RS on the ultimate strength of columns with slenderness of 40 under small eccentricity, especially for $0.7 < \varepsilon_0 < 4.5$. The different stress states of midheight cross section between the two columns may give a reason for such deviation in $\Delta N - \varepsilon_0$ curves. (1) For columns with slenderness of 70, the middle fiber strains (S02 and S05 in Fig. 8.16) of midheight cross section reach about 75% of f_y/E near peak load. Before peak load, we have $\left|\left(N/Af_y\right) - \left(z\Phi E/f_y\right)\right| < 1$, where Φ is the curvature at midheight. The superimposition of compressive RS may result in $\left|\left(N/Af_y\right) - \left(z\Phi E/f_y\right) + \left(\sigma_{rc}/f_y\right)\right| > 1$. In this case the presence of RS accelerates the yielding process of compressive side that is detrimental to the ultimate bearing capacities of slender columns. (2) For columns with mediate slenderness of 40, the middle fiber strains of midheight cross section are much higher than those of slender columns that are about 90% of f_y/E near peak load. The fibers in compressive side should have yielded under combined bending and axial compression, $\left|\left(N/Af_y\right) - \left(z\Phi E/f_y\right)\right| > 1$. However, the presence of tensile RS in the corners results in $\left|\left(N/Af_y\right) - \left(z\Phi E/f_y\right) + \left(\sigma_{rt}/f_y\right)\right| < 1$. Thus the corners are still in elastic status and able to provide additional bending resistance rather than the cross section without RS.

8.3.2.3 Effect of width to thickness ratio

Fig. 8.28 shows that the calculated interaction buckling curves with different d/t ratios differ from each other.

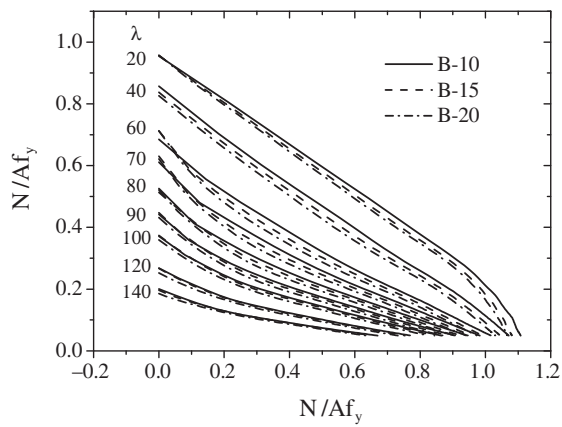

Figure 8.28 Comparison of interaction curves with varying d/t.

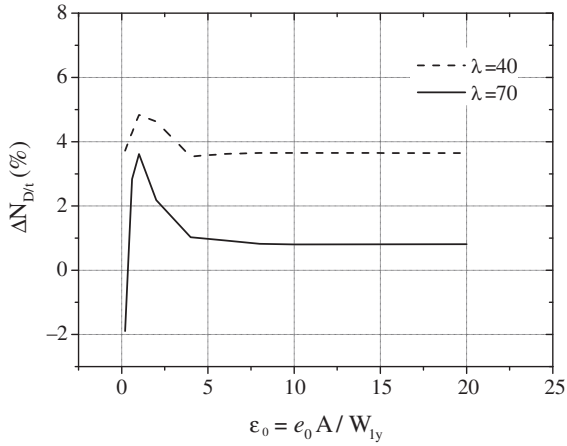

Figure 8.29 Strength difference between columns with d/t ratios of 10 and 20.

To evaluate the influence of d/t ratio, the strength difference versus eccentricity ratio curves is shown in Fig. 8.29. The strength difference between columns with d/t ratios of 10 and 20 is defined as:

$$\Delta N_{D/t} = \frac{\mathrm{N}_{B\text{-}10} - \mathrm{N}_{B\text{-}20}}{\mathrm{N}_{B\text{-}10}} \times 100\% \tag{8.14}$$

where $\mathrm{N_{B\text{-}10}}$ and $\mathrm{N_{B\text{-}20}}$ are the predicted ultimate strength of columns with d/t ratios of 10 and 20, respectively. The indirect influence of width to thickness ratio on the buckling behavior is derived from the effect of RS. The magnitude of the compressive residual stress ratio β decreases with the increase in d/t ratio, while the tensile residual stress ratio α is proportional to d/t ratio. Under small load eccentricity with $\varepsilon_0 < 5$, the effect of d/t is as same as discussed in Section 5.3. However, under large load eccentricity with $\varepsilon_0 \geq 5$, it is different from the case of under small load eccentricity. In addition to the compression side the fibers in the tension side have yielded before peak load, $\left|\left(N/Af_y\right) + \left(z\Phi E/f_y\right)\right| > 1$. The presence of compressive RS delays the yielding of fibers in tension side, $\left|\left(\mathrm{N/Af_y}\right) + \left(z\Phi E/\mathrm{f_y}\right) + \left(\sigma_{rt}/\mathrm{f_y}\right)\right| < 1$. The higher magnitude of compressive RS ratio is, the more beneficial to the ultimate strength of columns will be. This is the reason that the interaction curves of the B-10 series are higher than those of the B-20 series under large load eccentricity.

8.4 Design recommendation

8.4.1 H-sections

In this section the applicability of design rules given in EN 1993-1-1, ANSI/AISC 360-16, and GB 50017-2003 for Q690 steel columns of welded H-sections

under combined compression and bending is assessed by means of the ratios of the FE to design buckling resistances. In these design rules, effects of axial compression and bending moments are summed up linearly, while nonlinear effects of applied bending moments are accounted for by interaction factors. Since torsional deformation is beyond the scope of this research, factors related to torsional deformation were taken to be 1.0 in the calculation of design buckling resistances.

Large numbers of FE models for Q690 steel columns of welded H-sections under combined compression and uniaxial bending were established with variations in cross section sizes, nondimensional slendernesses, and initial loading eccentricity ratios. Cross section sizes included Sections H1, H2, H3, and H4 and nondimensional slendernesses included 0.6, 1.0, 1.4, and 1.8. Initial loading eccentricity ratios varied from 0.0 to 20.0. A total of 15 initial loading eccentricities were adopted, which were 0.0 to 1.0 with an interval of 0.2 and 1.5, 2.0, 3.0, 4.0, 5.0, 6.0, 8.0, 10.0, and 20.0. Residual stresses were incorporated in FE models. Initial out-of-straightnesses were taken to be sinusoidal shapes. The amplitudes of initial out-of-straightnesses complied with the theoretical background of corresponding design rules. In the assessment of both EN 1993-1-1 and GB 50017-2003, the amplitudes were 1/1000 of effective lengths, while for ANSI/AISC 360-16 the amplitudes were 1/1500 of effective lengths.

8.4.1.1 EN 1993-1-1

According to EN 1993-1-1, the buckling resistance for a steel member under combined compression and bending should satisfy the following equations:

$$\frac{\mathrm{N_{Ed}}}{\chi_{\mathrm{y}}\mathrm{N_{Rk}}/\gamma_{\mathrm{M1}}}+k_{\mathrm{yy}}\frac{\mathrm{M}_{y,\mathrm{Ed}}+\Delta M_{y,\mathrm{Ed}}}{\chi_{\mathrm{LT}}\left(\mathrm{M}_{y,\mathrm{Rk}}/\gamma_{\mathrm{M1}}\right)}+k_{\mathrm{yz}}\frac{\mathrm{M}_{z,\mathrm{Ed}}+\Delta M_{z,\mathrm{Ed}}}{\mathrm{M}_{z,\mathrm{Rk}}/\gamma_{\mathrm{M1}}}\le 1 \tag{8.15}$$

$$\frac{\mathrm{N_{Ed}}}{\chi_{\mathrm{z}}\mathrm{N_{Rk}}/\gamma_{\mathrm{M1}}}+k_{\mathrm{zy}}\frac{\mathrm{M}_{y,\mathrm{Ed}}+\Delta M_{y,\mathrm{Ed}}}{\chi_{\mathrm{LT}}\left(\mathrm{M}_{y,\mathrm{Rk}}/\gamma_{\mathrm{M1}}\right)}+k_{\mathrm{zz}}\frac{\mathrm{M}_{z,\mathrm{Ed}}+\Delta M_{z,\mathrm{Ed}}}{\mathrm{M}_{z,\mathrm{Rk}}/\gamma_{\mathrm{M1}}}\le 1 \tag{8.16}$$

where $\mathrm{N_{Ed}}$, $\mathrm{M_{y,Ed}}$, and $\mathrm{M_{z,Ed}}$ are the design values of the compression force and the moments about the major (y) and the minor (z) axes along the member, respectively; $\mathrm{N_{Rk}}$, $\mathrm{M_{y,Rk}}$, and $\mathrm{M_{z,Rk}}$ are the characteristic values of resistances to compression force and the bending moments about the major (y) and the minor (z) axes, respectively; $\Delta M_{y,Ed}$ and $\Delta M_{z,Ed}$ are the moments due to the shift of the centroidal axes for Class 4 sections; χ_y and χ_z are the reduction factors due to flexural buckling about the major (y) and the minor (z) axes, respectively; χ_{LT} is the reduction factor due to lateral-torsional buckling; $\mathrm{k_{yy}}$, $\mathrm{k_{yz}}$, $\mathrm{k_{zy}}$, and $\mathrm{k_{zz}}$ are the interaction factors; and γ_{M1} is the partial factor for resistance of members to instability assessed by member checks.

In the first terms of Eqs. (8.15) and (8.16), the reduction factors, χ_y and χ_z, are related to the in-plane buckling behavior, and they are determined from the studies on columns under axial compression. In EN 1993-1-1, for welded H-sections made of 690 N/mm^2 steel, curves "b" and "c" are currently proposed to calculate column buckling resistances about major (y) axis and minor (z) axis, respectively. Based on the residual stress measurement and the test results, higher column curves may be applicable for designing Q690 steel columns of welded H-sections, and the assessment of higher column curves will be conducted later. In the second terms the reduction factor χ_{LT} is related to the lateral-torsional buckling behavior, and it was taken to be 1.0 in calculations of design buckling resistances.

The interaction factors k_{yy}, k_{yz}, k_{zy}, and k_{zz} in the second and the third terms can be obtained from two different approaches given in Annexes A and B, respectively. It should be noted that the main difference between these two approaches is the way of presenting different structural effects. Annex A emphasizes transparency, and each structural effect is accounted for by an individual factor. However, Annex B works with simplicity and allows some structural effects to be combined into a global factor. In this study the design rules given in Annexes A and B in EN 1993-1-1 for Q690 steel columns of welded H-sections are assessed. It should be noted that in Annex A the factor C_{mLT} and a_{LT} are also related to torsional deformation, and they were both taken to be 1.0. In Annex B, there are two sets of formulae for the calculation of interaction factors k_{ij}, one for members not susceptible to torsional deformations and the other one for members susceptible to torsional deformations. The former was adopted since the effect of torsional deformation was neglected.

For H-section about major axis the average ratios of FE to design buckling resistances by using curves "a" and "b" are summarized in Table 8.17. It is found that the average ratios using either curves "a" or "b" are slightly larger than 1.00 with standard variations smaller than 0.04. It means that both curves "a" and "b" could provide conservative predictions to buckling resistances about major axis. However, compared with curve "b," the ratios using curve "a" are closer to 1.00. Thus the design rules using curve "a" should be recommended owing to its advantage in safety and accuracy in estimating Q690 steel columns of welded H-sections under combined compression and major axis bending.

For H-section about minor axis the average ratios of FE to design buckling resistances by using curves "a" and "b" are summarized in Table 8.18. For Annex A, even though the average ratios using curve "b" are larger than 1.00, a few unconservative design results are observed in columns with nondimensional slendernesses of 0.6 and 1.0. The minimum value of all the ratios using curve b is 0.96. To the contrary, only a few unconservative design results are found when using curve "c," and the minimum value of all the ratios using curve "c" is 0.99. For Annex B a few unconservative design results are found when using either curve "b" or "c". Overall, the design rules using curve "c" should be proposed due to acceptable accuracy in designing Q690 steel columns of welded H-sections under combined compression and minor axis bending.

Table 8.17 Ratios of FE to design buckling resistances about major axis according to EN 1993-1-1.

H-section (major axis)	Curve "a"				Curve "b"			
	Annex A		Annex B		Annex A		Annex B	
	Average	Standard deviation	Average	Standard deviation	Average	Standard deviation	Average	Standard deviation
H1	1.02	0.02	1.04	0.02	1.06	0.03	1.09	0.02
H2	1.01	0.03	1.02	0.03	1.05	0.03	1.07	0.02
H3	1.04	0.02	1.05	0.02	1.07	0.03	1.10	0.02
H4	1.03	0.02	1.04	0.02	1.06	0.04	1.09	0.03

Table 8.18 Ratios of FE to design buckling resistances about minor axis according to EN 1993-1-1.

H-section (minor axis)	Design with curve "b"				Design with curve "c"			
	Annex A		Annex B		Annex A		Annex B	
	Average	Standard deviation	Average	Standard deviation	Average	Standard deviation	Average	Standard deviation
H1	1.02	0.03	1.06	0.04	1.05	0.04	1.11	0.04
H2	1.02	0.05	1.07	0.04	1.06	0.06	1.12	0.04
H3	1.04	0.04	1.09	0.03	1.08	0.06	1.14	0.04
H4	1.04	0.04	1.09	0.03	1.08	0.06	1.14	0.04

8.4.1.2 ANSI/AISC 360-16

According to ANSI/AISC 360-16, the buckling resistance for a steel member under combined compression and bending should satisfy the following equations:

$$\text{When}\ \frac{P_r}{P_c} \geq 0.2 \quad \frac{P_r}{P_c} + \frac{8}{9}\left(\frac{M_{rx}}{M_{cx}} + \frac{M_{ry}}{M_{cy}}\right) \leq 1.0 \tag{8.17}$$

$$\text{When}\ \frac{P_r}{P_c} < 0.2 \quad \frac{P_r}{2P_c} + \left(\frac{M_{rx}}{M_{cx}} + \frac{M_{ry}}{M_{cy}}\right) \leq 1.0 \tag{8.18}$$

where P_r is the design axial force, P_c is the axial buckling resistance, M_{rx} and M_{ry} are the design moments about the major (x) and the minor (y) axes, respectively, and M_{cx} and M_{cy} are the moment resistances about the major (x) and the minor (y) axes, respectively.

In the first terms of Eqs. (8.17) and (8.18), P_c is related to the in-plane buckling behavior, and it is determined from the studies on columns under axial compression. In this standard, there is only one column curve for the calculation of buckling resistances of all types of steel columns, and the applicability of this column curve will be examined later. In the second and third terms, M_{cx} is the lower value obtained according to the limit states of yielding, lateral-torsional buckling, and compression flange local buckling. In the calculation of M_{cx} herein, the limit state of lateral-torsional buckling was neglected. M_{cy} is the lower value obtained according to the limit states of yielding and flange local buckling.

For H-section about major axis the average ratios of FE to design buckling resistances by using curves "a" and "b" are summarized in Table 8.19. It is found that all the ratios are larger than 1.00 with standard deviations no greater than 0.05. The minimum value of all the ratios is 0.97. That means the design rules in ANSI/AISC 360-16 could provide accurate predictions to buckling resistances of Q690 steel columns of welded H-sections under combined compression and major axis bending.

For H-section about minor axis the average ratios of FE to design buckling resistances are summarized in Table 8.20. It is found that except Section H4, the average ratios for the rest sections are smaller than 1.00. The minimum value of all the ratios is 0.91. The main reason should be that only one column curve is adopted in

Table 8.19 Ratios of FE to design buckling resistances about major axis according to ANSI/AISC 360-16.

H-sections	Average	Standard deviation
H1	1.04	0.05
H2	1.04	0.04
H3	1.05	0.05
H4	1.06	0.04

Table 8.20 Ratios of FE to design buckling resistances about minor axis according to ANSI/AISC 360-16.

H-sections	Average	Standard deviation
H1	0.97	0.05
H2	0.98	0.05
H3	0.99	0.05
H4	1.01	0.04

this code, and this curve is the mean curve of the band for the group with the largest amount of data in Structural Stability Research Council (SSRC) column categories. Thus overestimation on buckling resistance of eccentrically compressed columns will occur when neglecting the resistance factors. Therefore the design rules in ANSI/AISC 360-16 should be arguably considered applicable for designing Q690 steel columns of welded H-sections under combined compression and minor axis bending.

8.4.1.3 GB 50017-2003

According to GB 50017-2003, the buckling resistance for a steel member under combined compression and bending should satisfy the following equations:

$$\frac{N}{\varphi_x A} + \frac{\beta_{mx} M_x}{\gamma_x W_x \left(1 - 0.8\frac{N}{N'_{Ex}}\right)} + \eta\frac{\beta_{ty} M_y}{\varphi_{by} W_y} \le f \tag{8.19}$$

$$\frac{N}{\varphi_y A} + \eta\frac{\beta_{tx} M_x}{\varphi_{bx} W_x} + \frac{\beta_{my} M_y}{\gamma_y W_y \left(1 - 0.8\frac{N}{N'_{Ey}}\right)} \le f \tag{8.20}$$

where N is the design value of the compression force, M_x and M_y are the design moments about the major (x) and the minor (y) axes, respectively, φ_x and φ_y are the reduction factors for flexural buckling about the major (x) and the minor (y) axes, respectively, φ_{bx} is the reduction factor for lateral-torsional buckling; $\varphi_{by} = 1.0$, $N'_{Ex} = \pi^2 EA/\left(1.1\lambda_x^2\right)$, $N'_{Ey} = \pi^2 EA/\left(1.1\lambda_y^2\right)$, λ_x and λ_y are the slendernesses for flexural buckling about the major (x) and the minor (y) axes, respectively, A is the cross-sectional area, W_x and W_y are the elastic moduli about the major (x) and the minor (y) axes, respectively, β_{mx} and β_{my} are equivalent moment factors for in-plane stability about the major (x) and the minor (y) axes, respectively, β_{tx} and β_{ty} are equivalent moment factors for out-of-plane stability about the major (x) and the minor (y) axes, respectively, γ_x and γ_y are plasticity adaptation factors for bending about the major (x) and the minor (y) axes, respectively, $\eta = 1.0$ for members susceptible to torsional deformation $\eta = 0.7$ for members not susceptible to torsional deformation, f design yield strength of the steel material, and E is Young's modulus of the steel material.

In the first terms of Eqs. (8.19) and (8.20), the reduction factors, φ_x and φ_y, are related to the in-plane buckling behavior, and they are determined from the studies on columns under axial compression. Curve "b" is recommended to calculate column buckling resistances of welded H-sections with steel grades no greater than Q420 steel. The assessment of the column curve "b" and the higher column curve "a" for designing Q690 steel columns of welded H-sections will be conducted later. In the second term of Eq. (8.19), the reduction factor φ_{bx} is related to the lateral-torsional buckling behavior, and it was taken to be 1.0 in calculations of design buckling resistances.

In this design code the cross-sectional plastic moduli are evaluated by the product of plasticity adaption factors and cross-sectional elastic moduli. For welded H-sections the plasticity adaption factors for major (x) and minor (y) axes bending are taken to be 1.05 and 1.20, respectively. That may lead to a partial use of plastic bending resistances of compact and noncompact sections.

For H-section about major axis the average ratios of FE to design buckling resistances by using curves "a" and "b" are summarized in Table 8.21. It is found that the average ratios using curve "a" are slightly larger than 1.00 with standard variations no greater than 0.04. The minimum value of all the ratios using curve "a" is 0.97. Noting that the selection of column curves in this code is based on the "mean value" criteria, slight unconservatism should be allowed. Therefore the design rules using curve a could provide accurate predictions to buckling resistances of Q690 steel columns of welded H-sections under combined compression and major axis bending.

For H-section about minor axis the average ratios of FE to design buckling resistances by using curves "a" and "b" are summarized in Table 8.22. All the average ratios using curve "a" are greater than 1.00 but the standard deviations approach 0.10. This is because some FE results are significantly higher than the design results using curve "a." All the average ratios using curve "b" are significantly larger than 1.10, and their standard deviations are relatively reduced. The minimum value of all the ratios using curve "b" is 0.98. Therefore the design rules using curve "b" could make predictions with satisfactory accuracy to buckling resistances of Q690 steel columns of welded H-sections under combined compression and minor axis bending.

Table 8.21 Ratios of FE to design buckling resistances about major axis according to GB 50017-2003.

H-sections	Design with curve a		Design with curve b	
	Average	Standard deviation	Average	Standard deviation
H1	1.07	0.04	1.12	0.02
H2	1.05	0.04	1.10	0.02
H3	1.08	0.03	1.13	0.02
H4	1.06	0.03	1.11	0.03

Table 8.22 Ratios of FE to design buckling resistances about minor axis according to GB 50017-2003.

H-sections	Design with curve a		Design with curve b	
	Average	Standard deviation	Average	Standard deviation
H1	1.06	0.10	1.11	0.08
H2	1.07	0.09	1.11	0.07
H3	1.08	0.08	1.13	0.06
H4	1.08	0.08	1.13	0.06

8.4.2 Box sections

The interaction formula Eq. (8.21) is derived from the yield criteria of extreme edge fiber base on the elasticity assumption, which is in the form of the following equation:

$$\frac{N}{\chi_y A} + \frac{M_y}{W_{1y}(1-\chi_y(N/N'_{Ey}))} = f_y \tag{8.21}$$

To reflect the inelastic development of beam−columns in practice, it is rewritten in form of the following equation:

$$\frac{N}{\chi_y A} + \frac{\beta_{my} M_y}{\gamma_y W_{1y}(1-\eta_1(N/N'_{Ey}))} \le f_y \tag{8.22}$$

by introducing the inelastic development factor γ_y and the compensation coefficient η_1. The compensation coefficient of 0.8 is determined by the regression analysis of the numerical and experimental results of beam−columns with the nominal yield strength no more than 420 MPa. To this end, it is necessary to check whether it is suitable for HSS such as Q460C. The results of parametric analysis (N_{FE}) are compared with the interaction N_{GB} in GB 50017-2003, as summarized in Table 8.23, where $\varepsilon_{0,min}$ and $\varepsilon_{0,max}$ are the eccentricity ratios corresponding to the minimum and maximum values of N_{FE}/N_{GB}, respectively. The comparison shows that the current design code underestimates the ultimate strength of Q460C beam−column by 10%−18%.

To determine the compensation coefficient η_1 for Q460C welded box columns, a total of 2016 FE results are used in this study. Owing to the less sensitivity to RS and initial geometric imperfection of HSS columns, the recommended buckling curve "b" is adopted here for Q460C welded box columns [10]. The same value of inelastic development of 1.05 is adopted due to the good ductility of Q460C steel beam−column [12]. Hence, the compensation coefficient for Q460C welded box columns is obtained by regression analysis, which is 0.67. Table 8.23 shows the proposed modification of interaction formula ($N_{M,GB}$) agrees better with the FE

Table 8.23 Comparison of FE results and design code prediction.

Λ	Min (N_{FE}/N_{GB})	$\varepsilon_{0,min}$	Max (N_{FE}/N_{GB})	$\varepsilon_{0,max}$	Min ($N_{FE}/N_{M,GB}$)	$\varepsilon_{0,min}$	Max ($N_{FE}/N_{M,GB}$)	$\varepsilon_{0,max}$
10	1.05	0.2	1.12	0.6	1.05	0.2	1.12	1
20	1.08	0.2	1.15	1	1.05	0.2	1.13	1
30	1.11	20	1.16	1	1.04	0.2	1.11	2
40	1.11	20	1.17	2	1.03	0.2	1.10	2
50	1.12	20	1.19	0.2	1.03	0.2	1.11	4
60	1.11	20	1.23	0.2	1.03	0.6	1.09	6
70	1.12	20	1.26	0.2	1.02	1	1.08	6
80	1.11	20	1.26	0.2	1.03	1	1.09	0.2
90	1.10	10	1.24	0.2	1.03	2	1.10	0.2
100	1.10	20	1.23	0.2	1.03	2	1.10	0.2
110	1.10	20	1.20	0.2	1.03	2	1.09	0.2
120	1.09	20	1.18	0.2	1.03	2	1.08	0.2
130	1.09	20	1.15	0.2	1.03	2	1.07	0.2
140	1.10	20	1.14	0.2	1.03	2	1.05	0.2
150	1.10	20	1.14	0.2	1.03	4	1.05	0.2
160	1.10	20	1.13	1	1.03	4	1.04	0.2
Mean value	1.10		1.18		1.03		1.09	
Standard deviation	0.02		0.05		0.01		0.03	

results than the current design code. The underestimation of ultimate strength is reduced to 3%−9%.

8.5 Summary

Based on the studies hereinabove, the following remarks can be summarized as follows:

1. In the determination of design buckling resistances of Q690 steel columns of welded H-sections under combined compression and major axis bending, the design rules in EN 1993-1-1 using curve "a," and the design rules in ANSI/AISC 360-16 using the single curve, and the design rules in GB 5007-2003 using curve "a" are proposed;
2. In the determination of design buckling resistances of Q690 steel columns of welded H-sections under combined compression and minor axis bending, the design rules in EN 1993-1-1 using curve "c," the design rules in ANSI/AISC 360-16 using the single curve, and the design rules in GB 5007-2003 using curve "b" are proposed.
3. In the determination of design buckling resistances of Q460 steel columns of welded box-sections under combined compression and bending, the buckling curve "b," the inelastic development factor of 1.05, and the compensation coefficient of 0.67 are recommended according to the interaction formula in GB 50017-2003.

References

[1] Ma TY, Hu YF, Liu X, Li GQ, Chung KF. Experimental investigation into high strength Q690 steel welded H-sections under combined compression and bending. J Constr Steel Res 2017;138:449–62.

[2] Yan XL, Li GQ, Wang YB. Q460C welded box-section columns under eccentric compression. Proc Inst Civil Eng-Struct Build 2018;171(8):611–24.

[3] Ma TY, Li GQ, Chung KF. Numerical investigation into high strength Q690 steel columns of welded H-sections under combined compression and bending. J Constr Steel Res 2018;144:119–34.

[4] GB/T 1591-2008. High strength low alloy structural steels. 2008.

[5] European Committee for Standardization. CEN. EN 10025-6, Hot rolled products of structural steels-part 6: technical delivery conditions for fiat products of high yield strength structural steels in the quenched and tempered condition. Brussels: European Committee for Standardization; 2004.

[6] China Standard Press. GB/T 2975-1998 Steel and steel products: location and preparation of test pieces for mechanical testing. Beijing: China Standard Press; 1998 (in Chinese).

[7] National Standardization Technical Committees. GB/T 228-2002 Metallic materials: tensile testing at ambient temperature. Beijing: China Standard Press; 2002 (in Chinese).

[8] China Architecture & Building Press. GB 50017-2003. Code for design of steel structures. Beijing: China Architecture & Building Press; 2003 (in Chinese).

[9] European Committee for Standardization. CEN. Eurocode 3: Design of steel structures, Part 1-1: General rules and rules for buildings, EN 1993-1-1. Brussels: European Committee for Standardization; 2005.

[10] Wang YB, Li GQ, Chen SW, Sun FF. Experimental and numerical study on the behavior of axially compressed high strength steel box-columns. Eng Struct 2014;58(0):79–91.

[11] Wang YB, Li GQ, Chen SW. The assessment of residual stresses in welded high strength steel box-sections. J Constr Steel Res 2012;76:93–9.

[12] Wang YB, Li GQ, Cui W, Chen SW. Seismic behavior of high strength steel welded beam-column members. J Constr Steel Res 2014;102(0):245–55.